Process Status Evaluating Tool

How can the pump process status be evaluated pumping water?

M. De Bie

Faculty Offshore & Dredging Engineering

TU Delft Delft University of Technology

Challenge the future

PROCESS STATUS EVALUATING TOOL

HOW CAN THE PUMP PROCESS STATUS BE EVALUATED PUMPING WATER?

by

M. De Bie

Master of Science
in Offshore & Dredging Engineering

at the Delft University of Technology,

Student number: 4056450
Project duration: October 23, 2015 – January 31, 2017
Supervisor: Ir. K. Slager
Tu Delft Supervisors: Dr. Ir. A. M. Talmon
Prof. dr. Ir. C. van Rhee
An electronic version of this thesis is available at http://repository.tudelft.nl/.

TU Delft Delft University of Technology

PREFACE

Before you lies the thesis "How can the pump process status be evaluated?". This thesis is the start of the development of a *Proces Evaluation Tool*, which is part of the quest of Damen Dredging Equipment to make a CSD (cutter suction dredger) or DOP pump operable by everyone, for every slurry type, at correct working point every time. It has been written to fulfill the graduation requirements of the master Offshore & Dredging Engineering at TU Delft. I was engaged in researching and writing this thesis from November 2015 till January 2017.

This project did not only consist of analyzing data, but also of planning and performing new tests. To perform these test, I needed a short 'how to change an impeller of a centrifugal dredge pump'-course. Therefore I would like to thank everyone from the workshop at Damen Dredging Equipment for their daily guidance during four months, and for helping me whenever needed. Also I would like to thank my supervisor ir.K.Slager for his guidance during the whole thesis period.

Last but not least, I would like to thank the TU Delft supervisors dr.ir.A.M.Talmon & Prof.dr.ir.C.van Rhee for their visions and opinions which gave me other points of view on how to tackle the problems and how to properly communicate my findings.

I hope you enjoy your reading.

M. De Bie
Nijkerk, January 2015

ABSTRACT

Damen Dredging Equipment (DDE) has a quest to make their cutter suction dredger (CSD) and their DOP pump operable by everyone for every slurry type at the correct working point every time. To complete this quest, first a process status evaluating tool has to be developed which replaces the visual wear inspection. This thesis is the first step in developing this tool, its research question hence is "How can the pump process status be evaluated pumping water?"

To answer this question, first a literature study about a centrifugal pump is done (chapter 1) to understand the working principle of a centrifugal dredge pump. Next, the wear locations in a centrifugal dredge pump are going to be examined (chapter 3) after a small wear definition introduction (chapter 2). From the wear locations found, the ones that are expected to have the most influence on the pump performance (head H and efficiency η) are further researched in this thesis. These locations are: the axial gap and the inner impeller diameter. For the axial gap, data was already available due to previous research at DDE [1]. The data for the influence of the inner impeller diameter change is created by own experiments on the sediment transport circuit at DDE, these experiments are explained in chapter 5. Also another condition monitoring option (not only the influence of the pump parameters) is researched after different possibilities were investigated (chapter 4). This method is the vibration analysis of the pump and is used to see whether or not the influence of wear on the pump can be monitored. This wear is created by pumping a slurry (sand-water) mixture through the sediment transport circuit while using casted steel for the impeller and wear plate (it would take a lot of time to create wear on the original nihard impeller and wear plate).

The data for the axial gap, inner impeller diameter and vibrational analysis is explained in chapter 6. The research question can be answered in two parts: the influence on the pump parameters and the vibration analysis of the pump. The data analysis of the influence of the axial gap on the pump parameters (section 6.1) shows that it is possible to indicate whether the axial gap is small or large ($2mm$ vs $11mm$) by using a trial-and-error method proposed in this study. The data analysis of the inner impeller diameter (section 6.2) shows two methods to calculate the inner diameter increase from the data obtained during the own experiments. Both methods are based on the change of the velocity triangles resulting in an extended version of the pump affinity law for head. The $NPSH$ could not be measured decent, so no model is obtained for this. The last part to answer the research question is the vibrational analysis (in radial, axial and tangential direction). The BEP point can be found using the vibrational analysis (lower vibration level). Also cavitation in the pump is detected by the vibrational analysis (high scattering of vibrational data points). A last thing that can be seen is when the pump operates left from the BEP, the axial vibration level increases a lot.

All the findings in chapter 6 should be tested for not only the DOP250, but for a various range of pumps and settings. This to conclude if the findings are applicable for every pump, or only for the DOP250 in setting used in the sediment transport circuit.

CONTENTS

List of Figures

NOMENCLATURE

SYMBOLS

ROMAN

Symbol	Units	Description
$A_{1,2}$	m^2	Inner, outer circumferential area of the impeller
$b_{1,2}$	m	Inner impeller width at the inlet, outlet
$C_{1,2}$	m/s	Absolute velocity at the inlet, outlet
$C_{1,2m}$	m/s	Meridional velocity at the inlet, outlet
$C_{1,2U}$	m/s	Tangential part of the relative velocity at the inlet, outlet
C_M	–	Non-dimensional torque coefficient
C_{Q_L}	–	Contraction coefficient
C_{MDB}	–	Own empirical factor to fix the difference between $\eta_{Measured}$ and η_{model}
$D_{1,2}$	m	Inner, outer diameter of the impeller
D_{eff}	m	Effective diameter, difference between outer and inner diameter
D_{in}	m	Inner diameter impeller
D_{out}	m	Outer diameter impeller
f_D	–	Darcy friction factor
g	m/s^2	Gravitational acceleration
H	Pa	Head
H_{DF}	Pa	Head loss due to disk friction
$H_{Theoretical}$	Pa	Theoretical head created by the pump
$H_{recirculation}$	Pa	Head loss due to recirculation
$H_{measured}$	Pa	Head measured during the test at the sediment transport circuit
h	m	Geodetic position, distance from the reference axis
h_p	m	Geodetic position from the pressure sensor at the pump outlet to the pump axis
h_s	m	Geodetic position from the pressure sensor at the pump inlet to the pump axis
hp_d	W	Power absorbed by disk friction
K	–	Experimental factor
k_s	–	Surface roughness coefficient
L	m	Pipe length
M	$N \cdot m$	Moment/torque
$NPSH_A$	Pa	Net Positive Suction Head Available
$NPSH_R$	Pa	Net Positive Suction Head Required
$NPSH_{3\%}$	Pa	Net Positive Suction Head at 3% head loss
n	RPM	Rounds per minute
P_{hydr}	W	Hydraulic power
P_{shaft}	W	Shaft power
P_1	W	Pump power at n_1 RPM
P_2	W	Pump power at n_2 RPM
P_p	Pa	Pressure at the pump outlet
P_s	Pa	Pressure at the pump inlet
P_{man}	Pa	Manometric pressure from the pump

P_{vap}	Pa	Vapour pressure, temperature depending
P_{inlet}	Pa	Pressure at the inlet of the pump, a certain distance (L) from the pump inlet
P_{loss}	Pa	Pressure loss over a certain pipe length (L)
p	bar	pressure
$\triangle p_{tot}$	Pa	Total pressure difference
Q	m^3/s	Flow rate
Q_L	m^3/s	Volumetric flow rate loss
Q_{imp}	m^3/s	Flow rate from the impeller
$Q_{hydraulicoil}$	m^3/s	Flow rate from the oil in the hydraulic hoses
$R_{1,2}$	m	Inner, outer radius of the impeller
Re	–	Reynolds number
s	m	Axial gap width
s_{ax}	m	Axial gap width
$U_{1,2}$	m/s	Tangential velocity at the inlet, outlet
v_f	m/s	Fluid velocity
V_p	m/s	Fluid velocity at the pump outlet
V_s	m/s	Fluid velocity at the pump inlet
$W_{1,2}$	m/s	Relative velocity at the inlet, outlet

GREEK

Symbol	**Units**	**Description**
$\alpha_{1,2}$	°	Absolute flow angle at the impeller inlet, outlet
$\beta_{1,2}$	°	Relative flow angle at the impeller inlet, outlet
δ	m	Boundary layer thickness
η	%	Efficiency
η_{model}	%	Efficiency created by a model
η_{model1}	%	Efficiency created by an updated model
$\eta_{Measured}$	%	Measured efficiency from test in sediment transport circuit
ρ	kg/m^3	Fluid density
ρ_f	kg/m^3	Fluid density
ρ_m	kg/m^3	Pumped medium density
ω	rad/s	Angular velocity

ACRONYMS

AE	Acoustic Emission
BEP	Best Efficiency Point
CM	Condition Monitoring
DDE	Damen Dredging Equipment
DGV	Dredge Gate Valve
DOP250	DOP Submersible Dredge Pump 250
IT	Infrared Thermography
NDT	Non Destructive Testing
RPM	Rounds Per Minute
TDS	Tonnes Dry Solid

INTRODUCTION

BACKGROUND

The behaviour of dredge pumps is influenced by a couple of process parameters e.g. particle size & density and wear. The dredge pump end-user is mostly not aware of the relationship between wear and the pump performance/behaviour. It would be ideal if the end-user would use the pump around its Best Efficiency Point (BEP), because a large deviation could increase wear and therefore reduces the product lifetime. For every situation (different grain size, slurry density, pump wear, etc.) there will exist a work point with the lowest wear rate. Therefore the ultimate goal is to find an algorithm/tool/program that will control the pump to function at its most economical work point where the production is maximal while the energy consumption and wear rate are minimal. For this thesis a part of the *Process Status Evaluating Tool* will be researched from which the end-user can conclude whether the impeller or wear plate has to be replaced. This tool will replace a visual inspection which is time and money consuming. For this thesis the influence of the axial gap and inner diameter are researched.

The removal rate prediction is not part of this research since it is not asked for in the research questions. Hence making a prediction erosion model and researching anti-erosion measurements are not considered.

RESEARCH QUESTION

The assignment that was given by Damen Dredging Equipment (DDE) stated that a program or tool should be developed which could calculate the pump status from measured parameters. As already mentioned in Background (), this will be done during water circulation in the pump. Taking into account the grain size and slurry density would make the assignment even more difficult and its influence has therefore be investigated in a next research.

The main research question therefore is: *"How can the pump process status be evaluated pumping water?"*

OPERATIONALIZATION

The research takes place in Delft and Nijkerk (Damen Dredging Equipment). The location in Nijkerk is used for the weekly meetings, testing phase and whenever questions arise (proper mentoring is be available by my supervisor Ir.K.Slager). The location in Delft will be divided into two parts. The first part is the place where I conduct my research (Library, desk at home, etc.) and the meetings with the TU Delft supervisors Dr.Ir.A.M.Talmon & Prof.Dr.Ir.C.van Rhee.

IMPORTANCE

This research is assigned by Damen Dredging Equipment to increase the lifetime of the pump and to facilitate the indication when maintenance should happen and hence the pump should be opened for visual inspection or parts replacements. This will not only increase the product lifetime but also increase the total production per pump and make every pump more cost-effective, ergo make it more sustainable.

ROADMAP

To answer the research question, first a literature study (chapter 1) is done to understand how a centrifugal dredge pump works. The exact wear locations in the pump are examined (chapter 3) and discussed (to find the ones with the most influence) after wear is explained (chapter 2). This influence is always examined by comparing the different data for the pump parameters (manometric head H and efficiency η). In this thesis another condition monitoring method is discussed after a small research of different methods (chapter 4). After this, the experiments that are needed are determined (chapter 5) and their data analysed. These results will then be used to determine a wear prediction model for the investigated wear locations (chapter 6).

1

PUMP FUNDAMENTALS

The pump mostly used for dredging purposes, is the centrifugal pump. How a centrifugal pump transports slurry will be explained in section 1.1, together with its corresponding theory. In the other sections, section 1.2 & section 1.3, the possible wear locations and their influence and the pump condition monitoring options will be discussed respectively. The subjects tackled in this chapter are limited to the subjects needed for this research.

1.1. CENTRIFUGAL DREDGE PUMP

A centrifugal dredge pump differs with a normal centrifugal pump due to the transport of different types of slurry. A dredge pump has:

- Fewer number of blades: increase of maximum passage
- Larger gap between the tongue and impeller: to decrease the chance of rocks getting stuck in the volute
- Wear parts: easy replaceable parts.
- Protection of the drive shaft: keeping the shaft clean by injecting slurry-free liquid or by placing a mechanical seal in the gland.

1.1.1. PUMP COMPONENTS

The pump components and locations are shown in figure 1.1.

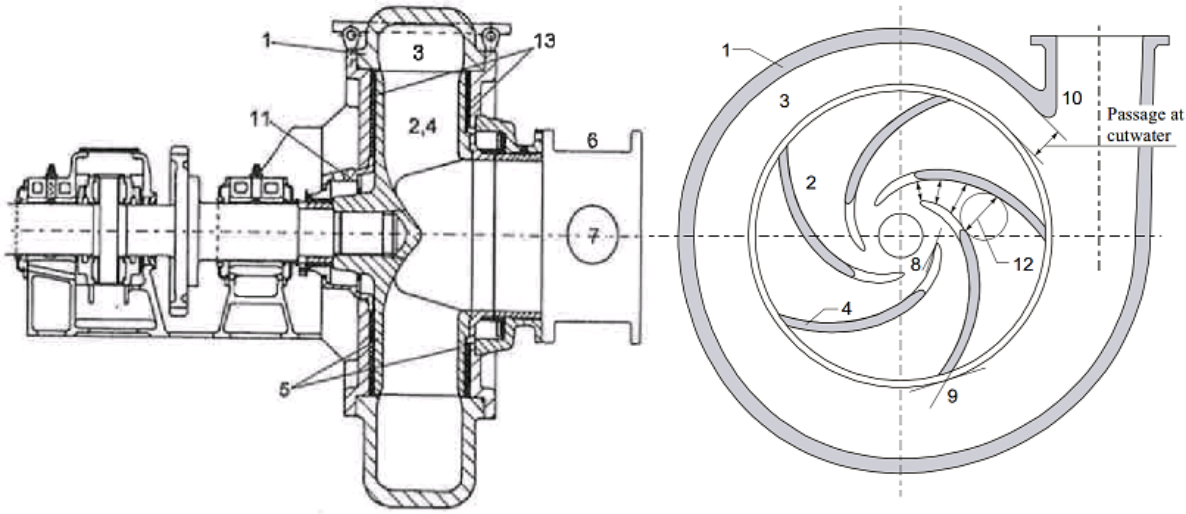

Figure 1.1: Dredge Pump Components and their Location [1]

1. Pump casing: Snail-shaped component in which the impeller turns.
2. Impeller: Two parallel shrouds with curved blades in between.
3. Volute: Open space between the impeller and pump casing.
4. Blade: Curved vane between the two shrouds.
5. Suction/Pressure Shroud: Front and back limitation of the impeller
6. Suction Bag: Flexible expansion piece made of rubber, also eliminates the vibrations between the suction pipe and pump.
7. Inspection cover: Cover on the suction side of the pump casing, to create the possibility to inspect the impeller.
8. Entrance angle: Angle at the beginning of the blade, flow accelerates from this point.
9. Exit angle: Angle at the end of the blade, flow leaves impeller at this point.
10. Tongue: Transition from pump casing to pressure pipe.
11. Gland: Slurry-free zone between shaft and impeller.
12. Maximum ball passage: Maximal ball diameter which can pass through the impeller blades.
13. Wear plate: Wear plates are removable components in the pump casing. These wear plates will reduce the amount of wear on the pump casing itself.

1.1.2. PUMP PARAMETERS

The most important pump parameters that where used in this report are shortly explained in this subsection.

HEAD (H)

According to [2], the head can be interpreted as the (mechanical) energy per unit gravity force (g). The Bernoulli equation (eq. (1.1)) quantifies this amount of mechanical energy available in a pipeline flow, which is constant at every location of the streamline. Therefore every term of eq. (1.1) is a different sort of head which is shown in fig. 1.2 and explained further below. In eq. (1.1), h is the geodetic position, p the pressure, v_f the fluid velocity and ρ_f the fluid density.

$$Level of Mech. Energy = h + \frac{p}{\rho_f g} + \frac{v_f^2}{2g} \tag{1.1}$$

Figure 1.2 represents a fluid flowing through a pipe section with a constant flow rate (steady) and density (incompressible). Two tubes can be seen in this pipe section: the piezometric tube (a) which measures the static pressure, and a pitot tube (b) which measures the manometric head (manometric head = static pressure + dynamic pressure = geodetic head + pressure head + velocity head). The fluid in tube b is higher in comparison with tube a, this can be explained using Bernoulli eq. (1.1) which is constant at every location on a streamline. The diameter of the pitot tube (and therefore the area) is a lot smaller in comparison with the pipe section. Therefore the velocity in the pitot tube will increase, resulting in the velocity head $\frac{v^2}{2g}$. The static head (tube a) consists of the pressure head $\frac{P}{\rho_f g}$ and the geodetic head h.

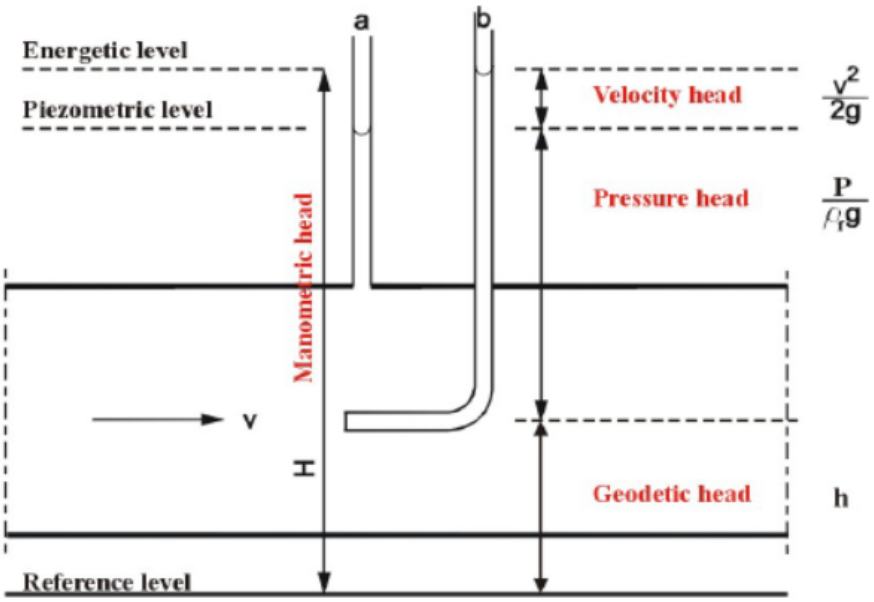

Figure 1.2: Different forms of head in Bernoulli equation [2]

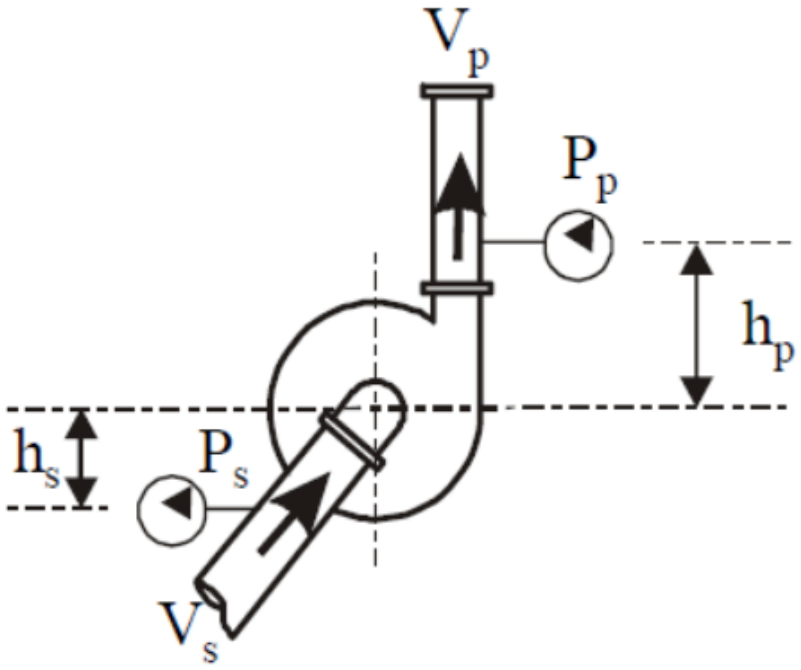

Figure 1.3: Conditions at inlet and outlet of a pump [2]

When applying eq. (1.1) to a centrifugal dredge pump (see fig. 1.3), it gives eq. (1.2). It is impossible to measure the exact manometric pressure at a location inside the pump, hence the configuration in fig. 1.3 is the most common one. The difference between two points (one at the inlet and one at the outlet) is taken with the pump axis as reference level.

$$P_{man} = \left(P_p - P_s\right) + \rho_m g \left(h_p + h_s\right) + \frac{\rho_m \left(V_p^2 - V_s^2\right)}{2} \tag{1.2}$$

All the pressures used in eq. (1.2) are absolute pressures , the pressures used are P_{man} (manometric pres-

sure), P_p (pressure at the pump outlet) and P_s (pressure at the pump inlet). Other parameters are: the vertical distance between the pump axis and the pump outlet (h_p) and between the pump axis and the pump inlet (h_s), the mean mixture velocity at the pump outlet (V_p) and at the pump inlet (V_s) and at least the density of the pumped medium (ρ_m).

EFFICIENCY (η)

Efficiency (η) is defined as the hydraulic power (P_{hydr}) divided by the power from delivered by the shaft (P_{shaft}).

$$\eta = \frac{P_{hydr}}{P_{shaft}} = \frac{\triangle p \cdot Q}{P_{Shaft}} \tag{1.3}$$

NET POSITIVE SUCTION HEAD ($NPSH$)

The absolute pressure inside the pump entrance should always be higher than the vapour pressure (the pressure at which the liquid boils). When the absolute pressure is lower, it means that the water starts boiling at that location, cavitation occurs. Cavitation will damage the pump and it will reduces the pump performance. At some locations inside the pump, the local pressure can be lower than the vapour pressure (P_{vap}) even if the pressure at the pump eye is larger than the vapour pressure. Therefore a safety margin has to be accounted for in the $NPSH_A$ or $NPSH_R$ definition.

- Net Positive Suction Head Available ($NPSH_A$): The total absolute pressure available at the pump entrance minus the vapour head ($\frac{P_{vap}}{\rho g}$) [10]. So the $NPSH_A$ is in fact the head that is higher than the vapour head, a sort of head surplus at the pump entrance.

$$NPSH_A = \frac{P_s}{\rho g} + \frac{V^2}{2g} + h_s - \frac{P_{vap}}{\rho g} \tag{1.4}$$

- Net Positive Suction Head Required ($NPSH_R$): is the minimum pressure required to prevent cavitation in the pump. The exact $NPSH_R$ cannot be predicted with precision, it must therefore be measured for the pump (see section 6.2.3).

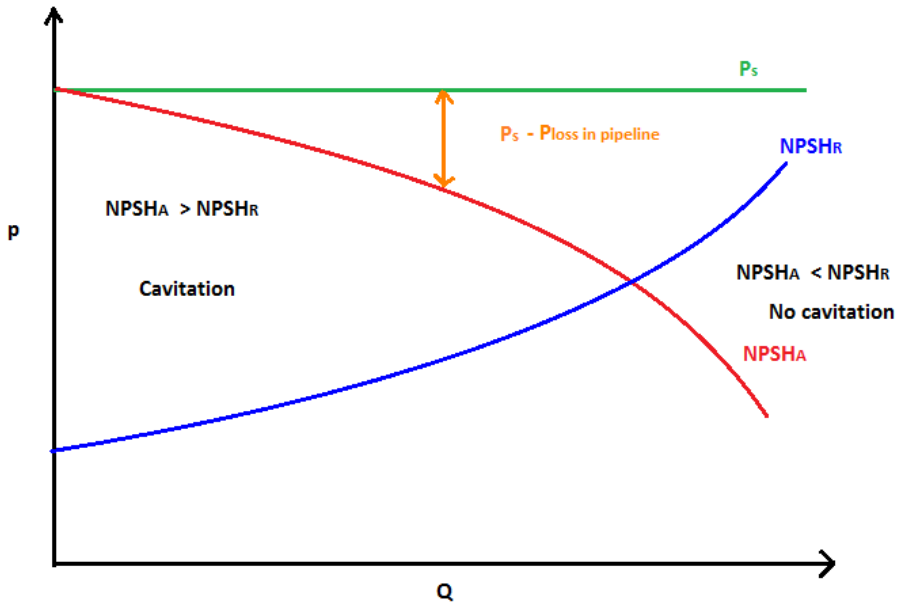

Figure 1.4: $NPSH_A$ vs $NPSH_R$ of a pump example

To prevent cavitation in every situation, eq. (1.5) should be maintained. This can be seen in fig. 1.4, it shows: the $NPSH_A$ curve (red), the $NPSH_R$ curve (blue) and the static pressure at the pump inlet sensor

P_s. The sensor is always located some distance (L) from the pump inlet, therefore the $NPSH_A$ curve shows a decreasing trend in comparison with P_s. This is due to the pipe resistance loss when increasing the flow rate and thus the velocity (V), $P_{loss} = f_D \frac{L}{D} \frac{1}{2} \rho V^2$. In which f_D is the darcy friction factor and D the inner pipe diameter.

$$NPSH_A > NPHS_R \tag{1.5}$$

PUMP CURVES

In fig. 1.5 the pump performance curves for the DOP250 from Damen Dredging Equipment (DDE) are shown for different RPM. Four different pump figures are visible: total head, power, efficiency and $NPSH_R$. The power used is not further discussed in this thesis since it was not possible to measure it. Every pump parameter is in function of the flow rate Q. The influence of the RPM can by explained by the affinity laws [10] with impeller diameter held constant:

$$\frac{Q_1}{Q_2} = \left(\frac{n_1}{n_2}\right) \tag{1.6}$$

$$\frac{H_1}{H_2} = \left(\frac{n_1}{n_2}\right)^2 \tag{1.7}$$

$$\frac{P_1}{P_2} = \left(\frac{n_1}{n_2}\right)^3 \tag{1.8}$$

P_1 is the pump power at n_1 revolutions per minute and P_2 is the pump power at n_2 revolutions per minute.

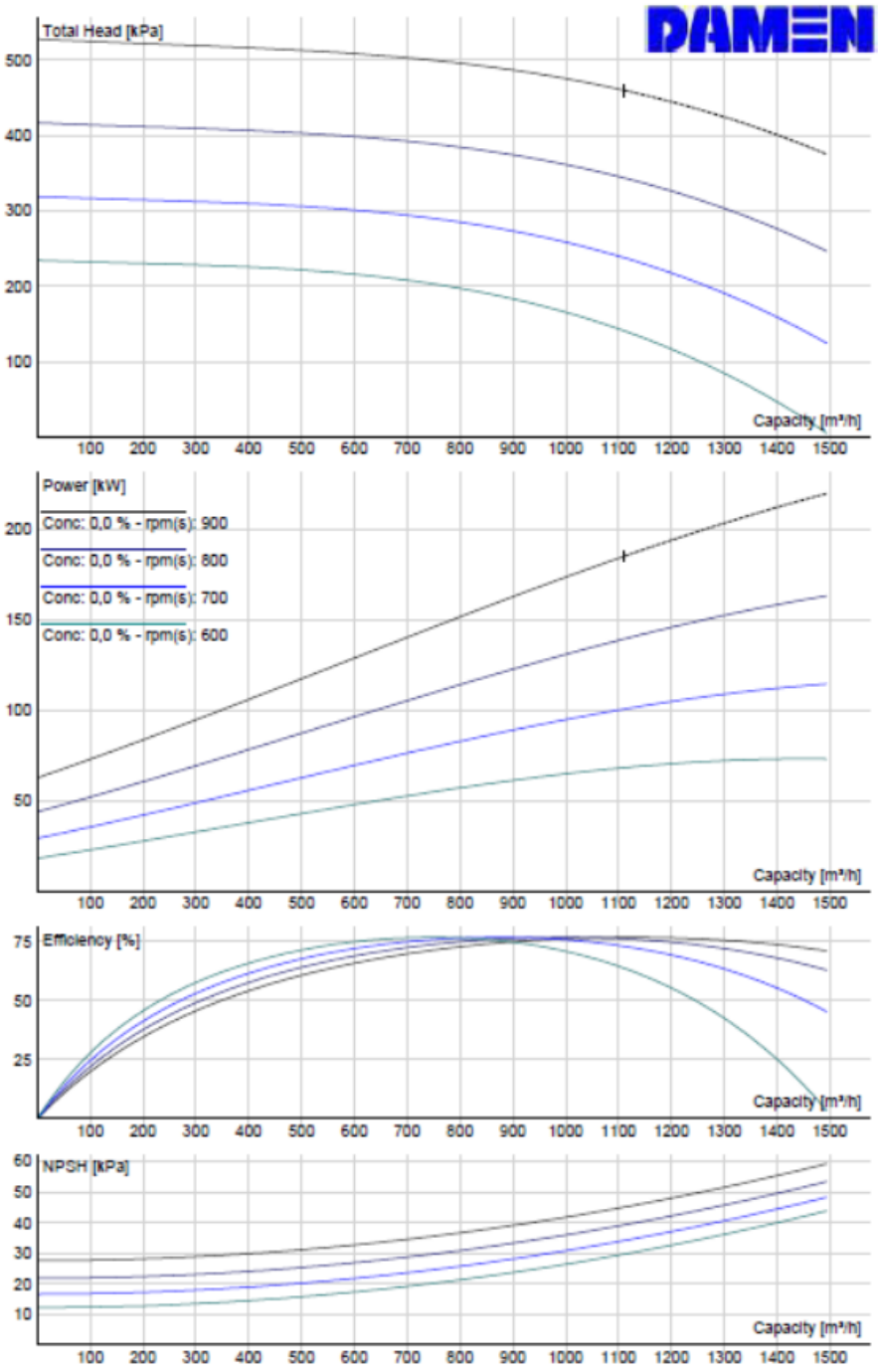

Figure 1.5: Pump Curves for Different RPM for a DOP250 Pump

1.1.3. WORKING PRINCIPLE

The centrifugal pump power is delivered by a drive-shaft. The rotational energy from this shaft is converted to kinetic energy of the fluid inside the pump. The fluid enters the impeller eye, the centrifugal forces created by the impeller pushes the fluid to the outer edges of the impeller into the volute. Doing this, the fluid gains velocity (kinetic energy) and also pressure (static energy) [3]. In the volute, the fluid is gathered and pushed further outwards into the pressure pipes by the snail-shaped pump casing (works as a diffuser). The theory of the working principle can be found in section 1.1.4.

1.1.4. PUMP THEORY

The purpose of this chapter is to explain the working principle by elaborating more on the theoretical part of the pump.

VELOCITY TRIANGLES

The flow through the impeller is a 3D-flow. To make it easier to understand the flow, a 2D representation is made by using velocity triangles as can be seen in fig. 1.6.

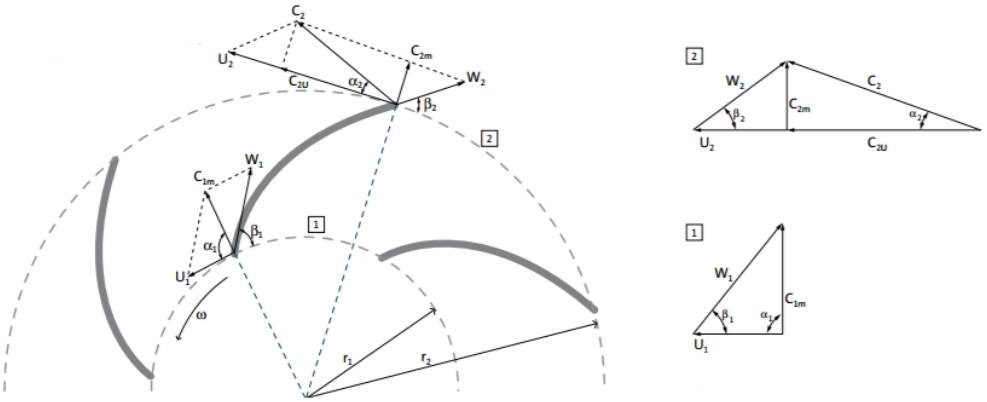

Figure 1.6: Velocity triangles positioned at the impeller inlet and outlet [3]

Fig. 1.6 shows the velocity triangles at their location in the impeller inlet (index 1) and impeller outlet (index 2). The velocity triangle at the outlet (index 2) consists of the absolute velocity C which is the sum of the relative velocity W and the tangential velocity U (eq. (1.9)). Also two angles are present: the relative flow angle β and the absolute flow angle α. The last velocity that can be seen is C_m, the meridional velocity.

$$\overrightarrow{C} = \overrightarrow{W} + \overrightarrow{U} \tag{1.9}$$

The difference between the velocity triangle at the inlet and the outlet is the absence of C. The flow is assumed to be stationary at the inlet, and at the stationary part of the pump, the absolute velocity C is equal to the relative velocity W [3]. Also it is assumed that there is no inlet rotation, so $C_1 = C_{1m}$ and $C_{1U} = 0$ [3].

Following formulas can be derived from the velocity triangles. Equations with both indices (1 and 2) can be used at the inlet and outlet. While only one index is used, the equation can only be used at only the inlet (index 1) or the outlet (index 2).

$$C_{1,2m} = \frac{Q_{imp}}{A_{1,2}} \tag{1.10}$$

$$A_{1,2} = 2\pi \cdot R_{1,2} \cdot b_{1,2} \tag{1.11}$$

$$U_{1,2} = 2\pi \cdot R_{1,2} \cdot \left(\frac{RPM}{60}\right) \tag{1.12}$$

$$\tan\beta_1, 2 = \frac{C_{1,2m}}{U_{1,2}} \tag{1.13}$$

$$W_2 = \frac{C_{2m}}{\sin\beta_2} \tag{1.14}$$

$$C_{2U} = U_2 - \frac{C_{2m}}{\tan\beta_2} \tag{1.15}$$

EULER PUMP EQUATION

The Euler pump equation, eq. (1.21), is derived by equalising the shaft power (1.16) and the hydraulic power (1.19). It can be equalised when it is assumed that there is no loss in the pump. The exact derivation can be found in Grundfos [3].

$$P_{shaft} = T \cdot \omega = m \cdot (U_2 C_{2U} - U_1 C_{1U}) \tag{1.16}$$

$$P_{hydr} = \triangle p_{tot} \cdot Q \tag{1.17}$$

$$H = \frac{\triangle p_{tot}}{\rho g} \tag{1.18}$$

$$P_{hydr} = Q \cdot H \cdot \rho \cdot g = m \cdot H \cdot g \tag{1.19}$$

$$P_{shaft} = P_{hydr} \tag{1.20}$$

$$H = \frac{(U_2 C_{2U} - U_1 C_{1U})}{g} \tag{1.21}$$

After applying the cosine equations to eq. (1.21), eq. (1.22) follows. This equation consists of 3 parts which each generate head, respectively: static head as consequence of the centrifugal force, the static head as consequence of the velocity change through the impeller and the dynamic head.

$$H = \frac{U_2^2 - U_1^2}{2g} + \frac{W_1^2 - W_2^2}{2g} + \frac{C_2^2 - C_1^2}{2g} \tag{1.22}$$

Considering the original Euler pump equation (eq. (1.21)) and assuming that there is no inlet rotation ($C_{1U} = 0$), results in eq. (1.23).

$$H = \frac{U_2 C_{2U}}{g} \tag{1.23}$$

Implement eq. (1.10) and eq. (1.15) into eq. (1.23), results in eq. (1.24). This equation shows the most important variables that influences the static head as a consequence of the centrifugal force with b_2 is the blade width at the blade exit.

$$H = \frac{{U_2}^2}{g} - \frac{U_2 Q_{imp}}{\pi D_2 b_2 g \tan \beta_2} \tag{1.24}$$

1.2. WEAR OCCURRENCE

The possible wear locations are examined and discussed in chapter 3, also the wear test locations are chosen in this chapter by the use of previous research [1]. No literature was available to determine these locations beforehand. The two locations that where chosen are the axial gap and the inner impeller diameter, these will be explained in the subsections below.

1.2.1. AXIAL GAP

The literature found related with the axial gap (disk friction and leakage) is explained, elaborated and referred to in section 6.1.

1.2.2. INNER DIAMETER

For the change in inner diameter, no exact literature was found. To understand the consequences of the inner diameter change, section 6.2 goes back to the pump basics and uses the velocity triangles from 1.1.4 to understand the consequences.

1.3. CONDITION MONITORING

Chapter 4 discusses the already existing condition monitoring tools, but also a few non-existing which could be plausible to use. These are explained and discussed in chapter 4. The literature used is also referred in this chapter.

2

WEAR

Wear occurs when a surface comes in contact with a slurry due to the speed difference of the surface and slurry. Two types of wear can be distinguished in a centrifugal dredge pump: hydroabrasive and cavitational wear. Hydroabrasive wear is of more general nature in comparison with cavitational wear. Therefore cavitational wear is not considered in this research since it is assumed that no cavitation occurs during normal operations. This assumption is in contrast with real life situation where cavitation is very likely to occur due to inexperience or wrong use of the end-user.

2.1. HYDROABRASIVE WEAR

The wear in a centrifugal dredge pump occurs at the flow-passage surfaces. This wear is caused by hydraulic abrasion in the pump. Hydraulic abrasion can be considered as a mechanical-abrasive process. The working fluid (slurry) consists of pure water and abrasive particles (e.g. sand). The effect of pure water on the surfaces of the flow-passage components is both mechanical and chemical (corrosive action), while the abrasive particles act only mechanical on these surfaces [4]. The action of the abrasive particles can be divided into two main categories: impact (2.1.1) and sliding abrasion (2.1.2), considering that particle wear is considered the primarily cause of wear in a dredge pump [4].

2.1.1. IMPACT WEAR

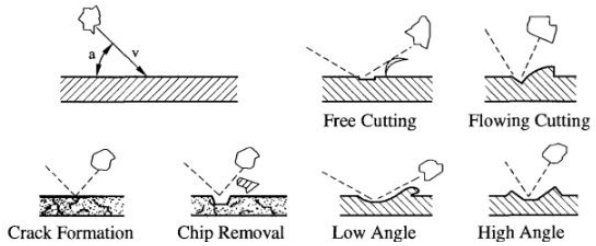

Figure 2.1: Impact Wear [4]

As can be seen in figure 2.1, the individual particles make contact with the surface with a certain velocity (V) and a certain angle of impact (α). Material removal occurs through the options shown in figure 2.1: individually (small scale deformation, fatigue cracking and cutting), or by a combination of those options. This depends upon the properties of the abrasive particles and the wear surface.

2.1.2. SLIDING WEAR

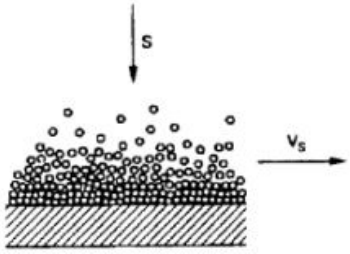

Figure 2.2: Sliding Wear [4]

Sliding wear can be seen as a bed of particles sliding against a surface tangentially with a certain bed load (s) and a velocity (V_s), as can be seen from figure 2.2. The material removal occurs through scratching of the surface, this can be compared to the free cutting from figure 2.1.

3

Wear Occurrence in a Centrifugal Dredge Pump due to Slurry Transport

The first step to answer the research question is to investigate the possible wear locations in a dredge pump, this is done by looking at the wear locations seen in practice and during previous research. Using an original impeller from Damen Dredging Equipment (*DDE*) would take too long to see the surfaces where erosion would occur. Therefore casted steel, another material compared to the one from *DDE*, was used. Casted steel is much softer which results in a higher erosion rate on the surfaces. To even further decrease the time needed to see the erosion, a sharp and rough sand was used with a large particle size e.g. crushersand.

The wear locations are examined, as already mentioned, during previous research [1]. During these tests, the pump has been opened to check the wear rate and the wear locations after 11.000 *TDS* (Tonnes Dry Solids) (fig. 3.4) and after 33.000 *TDS*. The pump casing is not discussed, it is assumed that the impact of its wear is negligible in comparison with the wear on the impeller and wear plate. Sealing components and bearings as well as inlet and outlet devices are not considered. Only measurable dimensions of the impeller and pump are taken into account. It is expected that every dimension of the impeller and wear plate will be subjected to wear. The wear rate will differ per location/dimension. These exact locations are shown and explained in their corresponding (sub)sections. These location are as follows:

- Wear plate (section 3.1)
- Wear on the impeller (section 3.2)
  - Wear on the suction shroud
  - Impeller outer diameter
  - Impeller inner diameter
  - Outer & inner blade width
- Blade thickness (subsection section 3.2.6)
  - Entrance angle
  - Exit angle
- Axial gap (section 3.3)

The causes and consequences for every wear location are discussed in the following (sub)sections. After this a conclusion about the wear locations that will be investigated more thoroughly is given.

3.1. WEAR ON THE WEAR PLATE

In fig. 3.1 an example of the location of the wear plate (*A*) is shown. This wear plate is mounted right behind the suction casing (*B*) of the dredge pump.

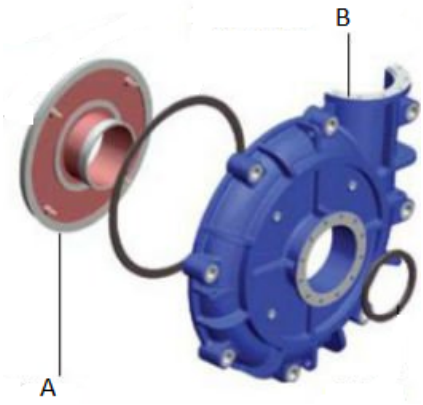

Figure 3.1: Wear Plate Location in Dredge Pump [5]

In fig. 3.2 the measurement locations for the wear plate are shown for a normal wear plate as in fig. 3.3. The consequences of local wear rate on the wear plate can be seen in fig. 3.4 The inner locations (1.1, 2.1, 3.1 & 4.1) and the outer locations (1.4, 2.4, 3.4 & 4.4) show the most wear, while the changes in the middle of the wear plate are almost nihil. This is due to the fact that the axial gap is larger in the middle and smaller at the inner & outer region. This phenomenon can be explained by disk friction: If the axial gap increases in size, the disk friction will decrease and therefore the wear rate will decrease. The wear pattern on the wear plate is the opposite of the geometry of the impeller shroud on suction side, fig. 3.13 shows clearly the suction shroud geometry.

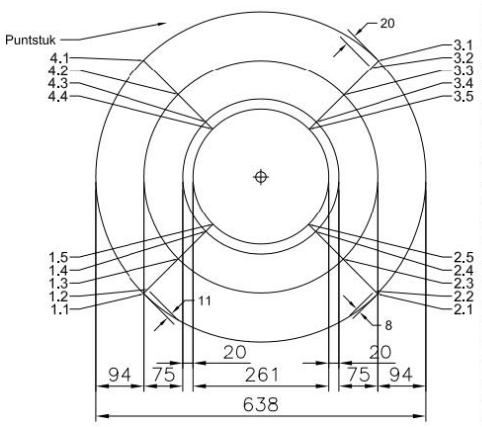

Figure 3.2: Wear Measurement Locations on the Wear Plate

Figure 3.3: Wear Plate after pumping 0 TDS

Figure 3.4: Wear Plate after pumping 11.000 TDS

3.2. WEAR ON THE IMPELLER

The wear on the impeller consists of wear on the inner & outer shrouds (outer diameter A, inner diameter B, impeller outer width C and the impeller blade width D (fig. 3.5) and on the blades entry & exit. The location where the wear occurs depend mainly on the velocity (RPM) of the impeller. Which will be explained in the section 3.2.1, section 3.2.6 & section 3.2.6.

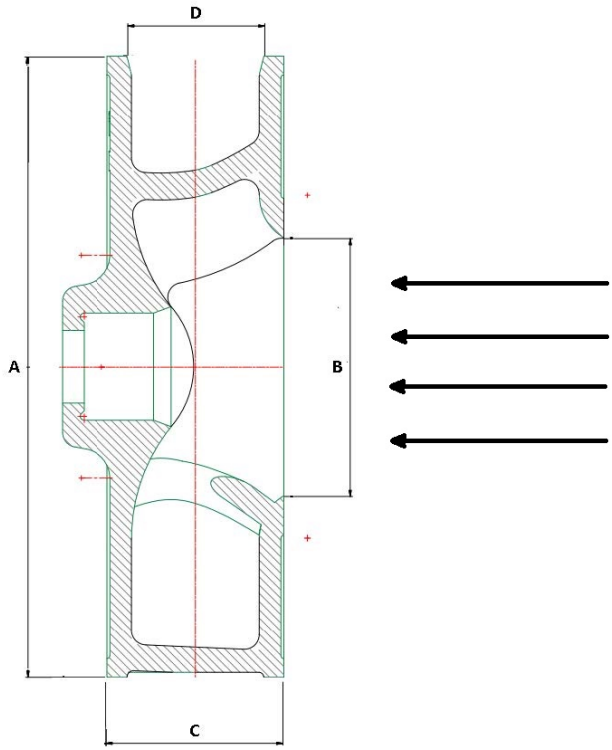

Figure 3.5: Impeller Shroud Wear Locations

3.2.1. WEAR ON THE SUCTION SHROUD

From previous research [1]: *A* decreases, *B* increases, *C* decreases and *D* increases in fig. 3.5, also the surface roughness decreases. The flow, in the axial gap on the suction side, is very turbulent, a lot of vortices and eddies are present, which results in a higher local wear rate.

3.2.2. *A*:OUTER DIAMETER IMPELLER

The outer edges of the blades and both shields are becoming thinner over time due to normal usage. After a certain time they will become so thin that it results in a decrease of the outer diameter. The wear rate of the shield diameter is higher in comparison with the place where the blades are located on the shield. This is normal because there is more material that has to be eroded, so it slows down the wear rate of the outer impeller at those places. When the RPM is kept constant, the head will decrease and therefore the work point will shift to a lower flow rate or with a higher impeller speed. This is also be seen by the pump affinity laws.

3.2.3. *B*:INNER DIAMETER IMPELLER

The inner diameter should be seen as a cylinder from the suction shroud till the pressure shroud. This cylinder can change its diameter along every point on the whole cylinder height (distance from suction to pressure side). The wear location along the height depends on the flow rate of the slurry. A higher flow rate (higher pipeline velocity) results in more wear towards the pressure shroud, while a lower flow rate results in more wear towards the suction shroud. This means that every impeller has an ideal flow rate for a specific slurry type, which will distribute the wear even over the blade width/cylinder height. The main consequence of increasing the inner diameter is that cavitation will occur faster. This occurs because of change in entrance angle and because of the increase of the inner diameter.

3.2.4. *C*:OUTER IMPELLER WIDTH

The decrease of the impeller outer width has an increase of the axial gap as result. Further information can be found in section 3.3.

3.2.5. *D*:BLADE WIDTH

The blade width is defined as the distance between the suction and pressure shroud. When the impeller wear is increasing over its lifetime due to normal pump usage, the blade width will become larger.

The head will therefore increase according to eq. (1.24). This equation is elaborated in section 1.1.4. In this equation (1.24, b_2 is the blade width). The head increase is almost negligible,it will increase with about $1kPa$ when the blade width increases with 10mm (660 RPM,pipeline velocity of 9.7 m/s). In practice this is the maximum reachable blade width.

3.2.6. BLADE THICKNESS

The blade thickness will be reduced during the impeller lifetime due to normal usage of the pump, the blade thickness decreases over the whole length. The consequences to the pump performance are assumed to be minimal. The efficiency would increase slightly due to the decrease of impact factor; the transition from the blade entry to the blade exit is smoother now.

WEAR ON THE BLADE ENTRY

During the first 11.000 TDS, in previous research [1], the flow rate was higher in comparison with the following 22.000 TDS. The higher flow rate is due to a higher RPM of the pump. The effect of the flow rate difference can be clearly seen after comparing fig. 3.6 & fig. 3.7 and fig. 3.7 & fig. 3.8. Using a higher RPM results in a higher wear rate in the back of the blades (pressure side), while a lower RPM results in a higher wear rate at the front of the blades (suction side). A general remark is the fact that the pressure side shows more wear than the suction side. This is logic, the flow is 'pushed' against it at a certain velocity.

The blades will become less thick over the total length (including blade exit) due to the tangential direction of the slurry over the blades. The effect of the blade wear on the pump behaviour is minimal, the efficiency will increase due to the decreased impact factor. Also the transition between the blade entry and exit becomes smoother, so less losses will occur.

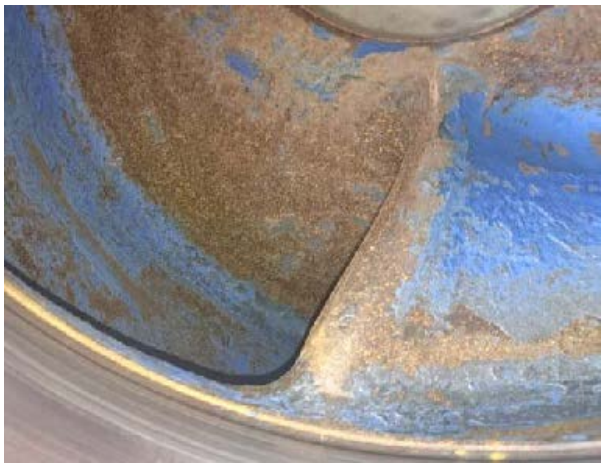

Figure 3.6: Blade Entry after pumping 0 TDS

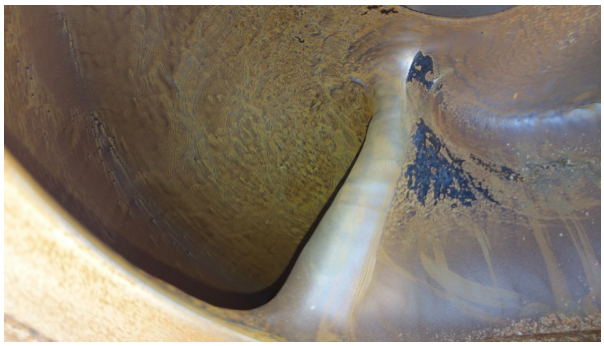

Figure 3.7: Blade Entry after pumping 11.000 TDS

Figure 3.8: Blade Entry after pumping 33.000 TDS

WEAR ON THE BLADE EXIT

The wear on the blade exit shows comparison with the wear at blade entry (section 3.2.6), in fig. 3.9, fig. 3.10 & fig. 3.11 this wear can be seen. The suction shroud is at the bottom in these figures.

Figure 3.9: Blade Exit after pumping 0 TDS

Figure 3.10: Blade Exit after pumping 11.000 TDS

Figure 3.11: Blade Exit after pumping 33.000 TDS

3.3. WEAR IN THE AXIAL GAP

An axial gap is the gap between the impeller and the pump housing. This means there are two axial gaps that could increase, one on the suction side and another one at the pressure side. These axial gaps are in contact with the volute so the slurry flows into these gaps. This flow and the related wear is initialised by the rotation of the disk and the related disk friction. This disk friction will cause wear on both the impeller and the pump housing at both sides (suction and pressure side). The shroud edges are becoming blunter and the axial gap increases, this can be seen when comparing fig. 3.12 and fig. 3.13. The wear rate on the pressure side is considered negligible since it is assumed that there is no slurry in the gland. There is a leakage from the axial gap on suction side to the suction entrance of the impeller. Because of this leakage, the wear rate will increase at the suction side and thus a wear plate is necessary to avoid to much wear on the pump housing at suction side. This axial gap increase results in a higher leakage rate which therefore results in an efficiency decrease. The increase of the axial gap can eventually result in an increase of almost 900% (increase of $20mm$) worst case scenario.

Figure 3.12: Suction Shroud after pumping 0 TDS

Figure 3.13: Suction Shroud after pumping 33.000 TDS

3.4. EXPERIMENT LOCATIONS CONCLUSION

From previous explanations, the choice has been made to investigate the influence of the axial gap on the suction side and the inner impeller diameter. These are expected to be the ones with the most influence on the pump performance and are possible to adjust by machining. Therefore they will be discussed more into detail when predicting a model for each wear location in chapter 6.

4

CONDITION MONITORING

In this chapter different condition monitoring solutions were investigated. These solutions are all Non Destructive Testing (NDT) solutions . In each section the NDT solution is explained and whether or not it is considered as a solution for this research. Not every solution si already existing, it can also be a plausible solution which came from a brainstorm session.

4.1. WIRES INSERTED IN THE WEAR PLATE

The electrical resistance of every wire is measured, the resistance changes with decreasing length/mass [11]. There are a couple of problems when implementing and using this wire technique. The first problem is the fact that the wear is not linear over the whole wear plate 3.4. So an in depth analysis should be made to the exact location where the wires should be inserted, but a possible wires placement is seen in fig. 4.1. In fig. 4.1, the black circle is the outer & inner edge of the wear plate wile the red circles are the wires placed on the wear plate and fig. 4.2 shows the placement of a wire inside the wear plate. Another problem is that the wires will change the flow across the wear plate. This will most likely introduce extra local vortices around the wires and therefore change the (local) wear rate.

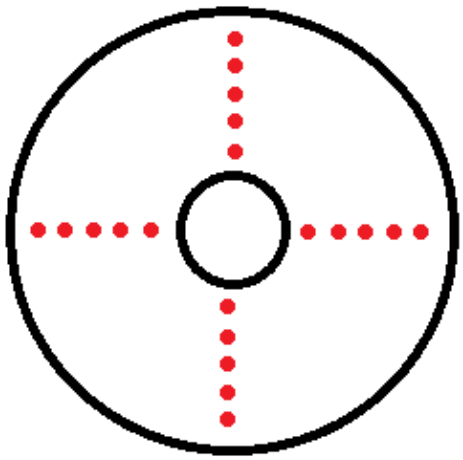

Figure 4.1: Possible Wires Placement on the Wear Plate

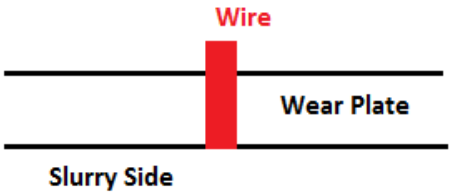

Figure 4.2: Wire Placement Inside The Wear Plate

4.2. INFRARED THERMOGRAPHY (*IT*)

Slightly variations in temperature across a surface can indicate failing of pump components e.g. bearings. The sensors can be placed at two different locations outside the pump: the wear plate and at the shaft bearings. The extra heat generated in the bearings can have a lot of causes (shaft misalignment, broken bearing, etc.). Heat differences at the wear plate surface can indicate a higher or lower local wear rate at the moment and not the total wear which is decisive for changing the impeller/wear plate. Therefore it is decided not to implement this method as an measuring method in this thesis.

4.3. ACOUSTIC EMISSION (*AE*)

Acoustic Emission (*AE*) tools are mostly designed for monitoring acoustic emissions during material failure instead of transmitting actively waves. Failure of pump components will be noticed after failure rather than before (which is what should be investigated in this thesis and thus needed). According to Sikorska [12], *AE* can be a more useful tool for analyzing hydraulic activity than traditional techniques. Hence using *AE* monitoring actively can detect both cavitation and recirculation rather easily at the moment it occurs. So for detecting only cavitation, this is the ultimate tool.

4.4. ULTRASONIC THICKNESS MONITORING (WEAR PLATE)

The wear over the whole wear plate is not linear 3.4. So an in-depth analysis should be made to the exact location where the thickness should be tested. After the thickness is measured, a relation still has to be determined between the wear plate and impeller wear rate. It is decided not to implement this condition monitoring method due to the availability of other more interesting options. This method has to be investigated in a further research.

4.5. PUMP PERFORMANCE MONITORING

Ideally there are five parameters that should be monitored to fully understand the pump performance: Head, $NPSH$, flow rate Q, pump speed and power. As the pump will wear, the power needed to achieve a certain suction/discharge pressure will increase. The key question is if it is possible to develop a model which is able to estimate the wear on the impeller/wear plate from the five parameters [13]. This will be researched by investigating the different wear locations independently. The different wear forms of the pump are all investigated independent of each other to exactly see their influence on the pump performance. From this a model is developed which should estimate the wear rate of each wear form. Different models will be combined into one model to determine the wear rate of the whole pump, verification (meet design specifications, theoretically) & validation (meet the design requirements, in practise) is therefore needed.

4.6. PUMP VIBRATION ANALYSIS

According to [13]; "vibration analysis is the cornerstone of all pump performance monitoring programs. The vibration level of a pump is directly related to where it is operating and in relation to its BEP. The further away from the BEP, the higher the vibrations will be. There is no absolute vibration amplitude level that is indicative of a pump in distress." Pump vibration analysis is easy to use for continuous condition monitoring and therefore spot problems before they even can happen. A simple warning light can indicate the excessive vibrations on the pump. It is not yet sure that vibration analysis will help to predict the pump wear, but it will definitely indicate other failure modes like pump imbalance, shaft looseness, cavitation, etc.

4.7. CONCLUSIONS

As already mentioned, the condition monitoring solutions that are used in the experiments are the pump performance monitoring (section 4.5) and the vibrational analysis (section 4.6). Their success rate were expected to be the highest.

5

EXPERIMENTS

In the test action plan all the needed info for the different tests and test set-ups are discussed. For every test the DOP250 pump from DDE is used. Its exact specifications can be found in appendix A. The data for the increase in axial gap was already available due to previous research [1], therefore it is not mentioned in this chapter.

5.1. OBJECTIVES

The first objective is to test the increase of the inner impeller diameter and check its influence on the pump performance parameters, as mentioned in chapter 4.5. The second objective is to test the influence of the wear on the pump performance parameters (exclude $NPSH$) and pump vibration, as mentioned in chapter 4.5 & 4.6. Further explanation of the exact scenarios needed to reach both objectives can be found in 5.5.1. In this subsection the exact test set-up can be found.

5.2. REQUIRED RESOURCES

The tests will be conducted in the sediment transport circuit at Damen Dredging Equipment (DDE) in Nijkerk. The impellers used are made of a different material than the original impellers used in the dredge pumps. They are made from a softer material (cast steel) to increase the wear rate and to make it easier to adjust the impeller to the different wear types that will be tested. These adjustments are machined at the workshop at DDE. To be able to change the impeller, the whole DOP250 pump is removed from the sediment transport circuit and transported to the workshop and vice versa after replacing the impeller. Sometimes the sediment transport circuit was not reachable by the Damen Multi Cat, so a crane was rented for installing and removing the DOP250 pump.

5.3. SEDIMENT TRANSPORT CIRCUIT

In a quest for product improvement DDE has designed and build a testloop in which a variety of dredging components can be exposed to heavy dredging conditions. This way components can be compared without having to utilize them during important projects, saving time and money. The main dimensions of this circuit are shown in fig. 5.1. The inner pipe diameter everywhere is $250mm$ (therefore the DOP250 is used in the circuit).

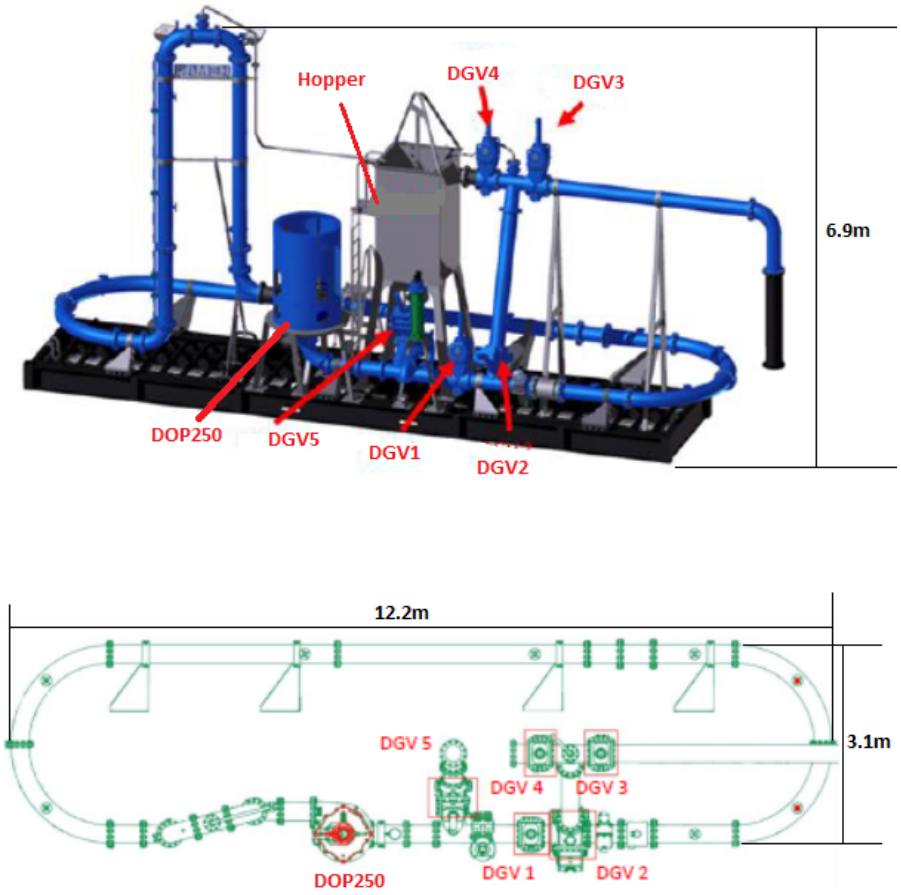

Figure 5.1: Sediment Transport Circuit

The main hardware components to control are the DGV (Dredge Gate Valve), Hopper (with moveable overflow) and the *DOP*250 pump. These are al shown in fig. 5.1. The flow and concentration of the mixture are controlled by regulating the DGV and hopper with its moveable overflow. The DOP250 pump is hydraulic driven by the power-pack, the 600DP power-pack from Damen is used. The sensors and their locations in the circuit are explained in section 5.3.1. A large U-bend can be seen in the circuit, this was originally implemented to be able to calculate the transport concentration of the circuit [10].

5.3.1. SENSORS

All the sensors used in the sediment transport circuit and their locations are explained below and also shown in fig. 5.2.

- PT001 & PT002: Vega pressure sensors (VEGABAR82). This type of sensor is an absolute pressure sensor with a measure range of 0-25 bar with an output signal of 0-20mA. The sensors are placed in front of the pump (PT001), and in the first vertical part of the U-bend directly after the pump (PT002). The exact locations are shown in fig. 5.2. The output signal (every second a signal) of these sensors are a time average of the last 3 seconds measured
- PT003 & PT004: Hydac pressure sensors that as a measure range of 0-400 bar with an output signal of 0-20mA. Their location is on the hydraulic block which is the connection between the engine and the hydraulic hoses.
- DT001:The volume concentration meter is meter with a radioactive source (Berthold SSC-100) and its measure range in this circuit is 1 - 1.8 ton/m^3. Its location is the yellow part in fig. 5.2.
- TT001: The temperature sensor used is a PT100 sensor. It has a measure range between $-200°C$ and $+850°$ and gives an output of 4-20mA. Its located in the vertical part of the U-bend after the DOP250.

The exact location can be seen in fig. 5.2.

- FT001: The flow sensor (blue in fig. 5.2 used is the Krohne Optiflux 4000 DN250. It's measure range variates from 0-10 m/s.
- RPM: The revolution counter is a proximity sensor which counts two pulses per revolution. The exact measure range is not known, but is sufficient for the RPM of the pump. The revolution counter is place on the shaft of the DOP250.
- Vibration sensor X, Y & Z: MTN 1185C series 4-20mA velocity transducer (the 4-20mA output is proportional to the rms velocity [mm/s]). These three sensors are mounted on the DOP250, an exact location and the axis definition can be found in fig. 6.25.

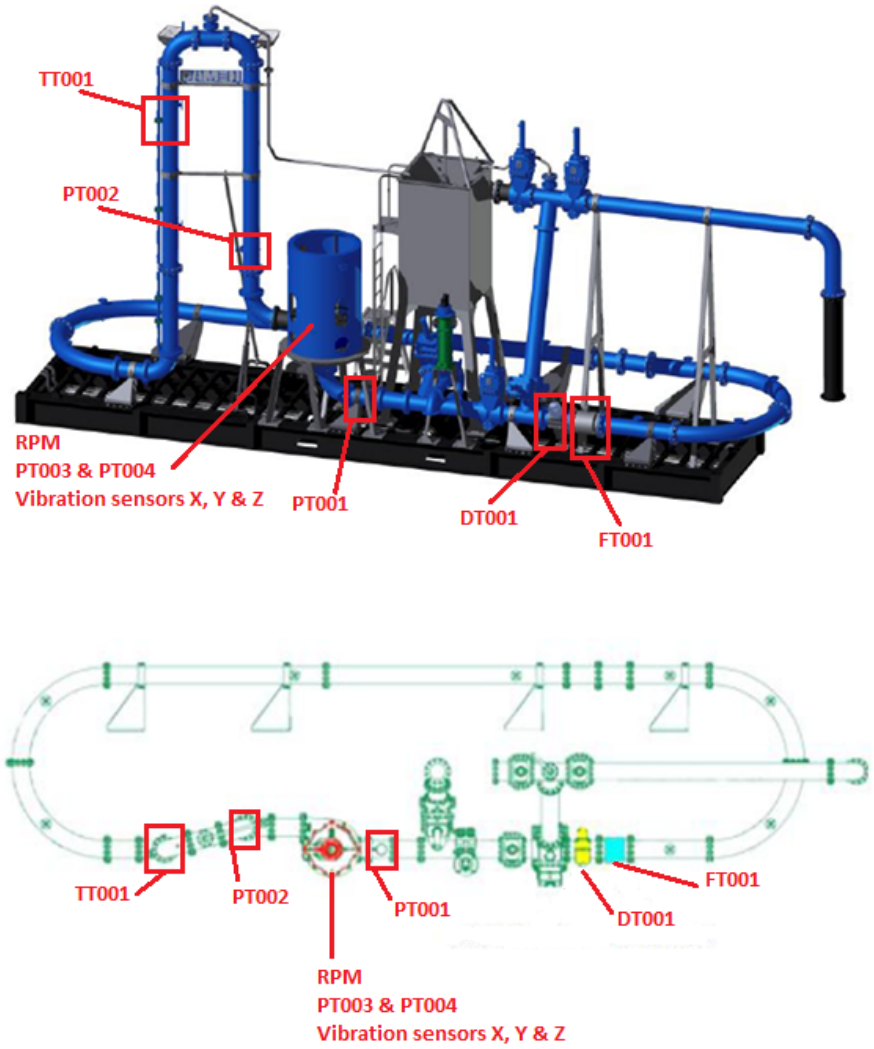

Figure 5.2: Sediment Transport Circuit Sensor placement

5.3.2. PUMP PARAMETERS IN THE SEDIMENT TRANSPORT CIRCUIT

In this subsection, a general explanation of how the pump curves (head and efficiency curves) and $NPSH$ curves are generated is given, while using the sediment transport circuit. For the experiments, the circuit is always filled with water and made air free.

PUMP CURVE

The general pump curve generated in the sediment transport circuit consists of a head and efficiency curve. The definition of both and their calculation are explained below. The easiest way to create the data for the

pump curves is via a closed system in which one DGV (DGV1) is available to regulate the flow rate. The circuit is closed by completely closing DGV2 and DGV5, their locations can be seen in fig. 5.1. The DOP250 is started and a RPM of 660 is set. A pump curve consists of at least 5 different measurement sets (see fig. 5.5 for definition of a measurement set), and each measurement set consists of at least 120 data points. The different measurement sets are created at different flow rates (Q), these flow rates are changed by closing DGV1 step by step. Closing DGV1 results in an increased pressure in front of DGV1 (and therefore at pressure sensor PT002), while the flow rate decreases.

Head

The head H generated in the sediment transport circuit is defined as the manometric pressure and is expressed in bar for the experiments. The manometric pressure is the difference between the absolute pressure before and after the pump. To this difference the influence of the height is added (+0.13 bar).

$$H = \triangle p + 0.13 = PT002 - PT001 + 0.13 \tag{5.1}$$

Efficiency

Efficiency (η) is defined as the hydraulic power (P_{hydr}) divided by the power delivered by the shaft (P_{shaft}). In eq. (5.4), $Q_{hydraulicoil}$ is the oil flow rate in the hydraulic hoses. The mechanical losses are included in efficiency since the sensors are located in the hydraulic block outside the DOP250 pump.

$$\eta = \frac{P_{hydr}}{P_{shaft}} \tag{5.2}$$

$$P_{hydr} = (PT002 - PT001 + 0.13) \cdot Q \tag{5.3}$$

$$P_{shaft} = (PT003 - PT004) \cdot Q_{hydraulicoil} \tag{5.4}$$

NPSH

To be able to generate the measurement sets as defined in section 6.2.3, the suction flow has to be varied for the same flow rate. Therefore two valves are needed (the valves are shown in fig. 5.1): one at the suction side (DGV5) to be able to decrease the pressure in front of the pump, and another at the pressure side (DGV2) to regulate the flow rate at which the measurement sets are generated. As already indicated DGV2 & DGV5 are used, this can only be done when DGV1 is closed. The circuit is considered 'open' since the flow in front of the pump has no initial velocity, the hopper functions as a basin from which the DOP250 pumps the water. Thy circuit is also exposed to atmospheric pressure. How the $NPSH_R$ is exactly calculated is explained in section 6.2.3.

5.4. RISKS & DEPENDENCIES

There are two main types of risk. One type of risk is about machining the wear types on the impeller. It is not yet known if it will be possible to machine the wear types, and which difficulties this will bring along. Another type of risk is about the measuring of the $NPSH$. During some previous research it was impossible to get a correct measurement due to a small air leakage trough one of the seals. The last mentioned risk in here is about the vibration sensors, this is not yet done before at DDE so it could bring along start-up problems. There are other risks present, but only the most important are mentioned.

5.5. TEST STRATEGY

The strategy for testing (pump behavior & vibrations) consists of a traceability matrix and the pass/fail criteria. In the traceability matrix, every test is explained by a matrix in which can be seen what exactly is tested in every test.

5.5.1. TEST TRACEABILITY MATRIX

The test traceability matrix (figure 5.3) shows what exactly is measured for every kind of test performed. Two main test are executed: the impeller inner diameter change (test 1) and the influence of pump wear on the pump vibration (test 2) For every start test (e.g. 1.1 & 2.1) the whole pump is renewed and a measurement is done with a new impeller and a new wear plate. This measurement is used as a baseline for the data analysis.

For test 2, the influence of pump wear on the pump vibration, the worn impeller from test 2.1.2 is used for test 2.2.1. The impeller from test 2.1.1 is worn during test 2.1.2 with a sand-water mixture. Normally test 2.1.1 and 2.1.2 would be repeated a couple times (resulting in 2.2.1, 2.2.2 and 2.3.1), but due to time constraints this was not possible. Therefore it was decided to perform test 2.1.2 as long as possible and create as much wear as possible. This to get a more clear result for the wear influence on the pump vibrations.

	Impeller used					Mixture used		Data obtained from test			
Test	Original Impeller	Din: original + 6mm	Din: original + 18mm	Din: original + 48mm	Worn impeller from previous test	Water test	Sand test	Pump Curve	Vibration monitoring	NPSH	Measure Dimensions
Test 1.1.1	X					X		X			
Test 1.1.2	X					X				X	
Test 1.2.1		X				X		X			
Test 1.2.2		X				X				X	
Test 1.3.1			X			X		X			
Test 1.3.2			X			X				X	
Test 1.4.1				X		X		X			
Test 1.4.2				X		X				X	
Test 2.1.1	X					X		X	X		
Test 2.1.2	X						X		X		X
Test 2.2.1					X	X		X	X		

Figure 5.3: Traceability Matrix

The results from the tests shown in fig. 5.3 are presented and explained in section 6.2 (test 1) and section 6.3 (test 2).

5.5.2. PASS/FAIL CRITERIA

The tests done fulfil the pass criteria. These criteria are summed below.

- The impeller and wear plate have to be in a new state, they should not be used before. (For baseline measurement)
- The pump parameters are measured in comparison to the flow rate.
- At least 5 measurement sets have to be performed to get a full coverage of the pump curves. An example of a measurement set is shown in fig. 5.5
- Each measurement set consist of at least 120 data points
- The pump runs at a constant RPM (660RPM)

- The measurements are performed with water ($1000 kg/m^3$)

Extra criteria for $NPSH$ measurement in 5.5.1:

- The flow rate is kept constant.
- At a 3% reduction of the manometric head, the $NPSH_R$ curve is established.
- A $NPSH_R$ consists at least of 3 different measurement sets at 3 different flow rates (Q).
- Each measurement set consists at least of 5 measurement points.

5.6. ANALYSING TEST RESULTS

The PLC-program used at the sediments transport circuit from DDE delivers the results from the tests as a $.CSV$-file, to make it easier to use the data a conversion program is available to convert these files into $.xls$-files. Every data point in these files is in fact an average over three seconds (see section 5.3.1). The data in the $.xls$-files is analyzed manually. First the points between the measurement sets are deleted. The not relevant points are the points produced between the measurement points used to make the pump curves. This can be seen when comparing fig. 5.4 and the orange data points in fig. 5.5. These points can be deleted because the flow is not considered steady and the data produced is therefore not useful (only the measurement sets are considered. The next step is to correct the data points by the affinity rules to a RPM of 660. The RPM is not constant during the test and varies with 5 to 10 RPM.

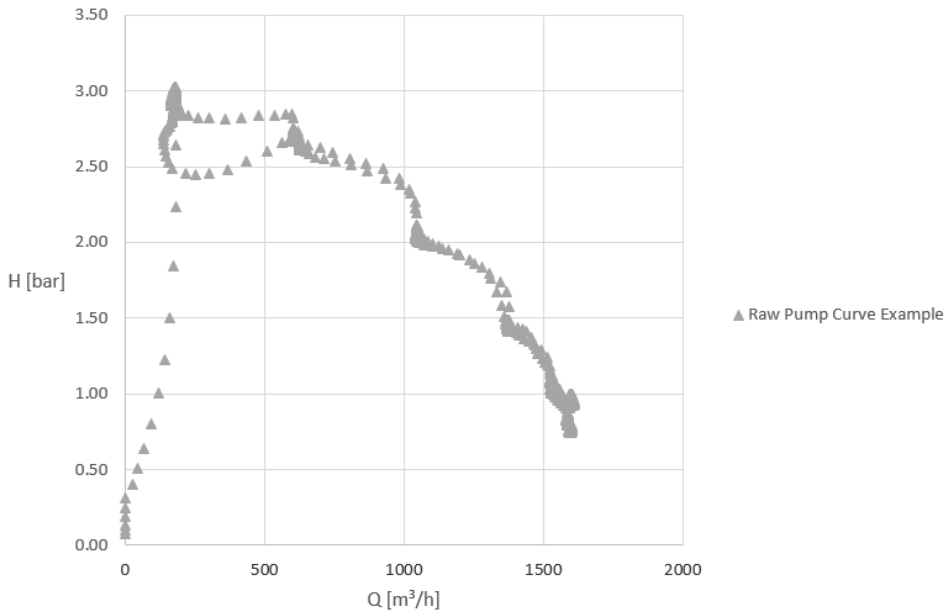

Figure 5.4: Raw Data Pump Curve Example

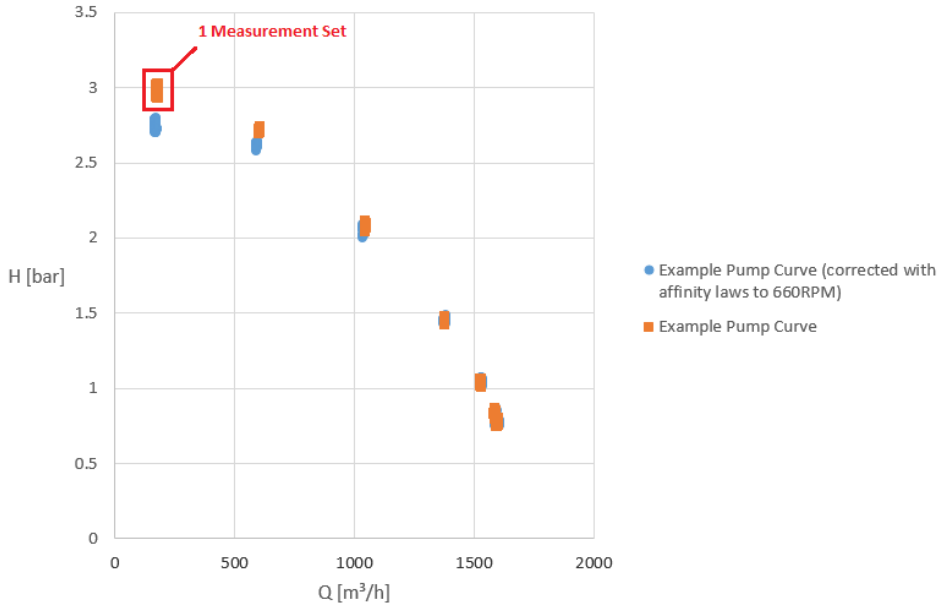

Figure 5.5: Pump Curve Example

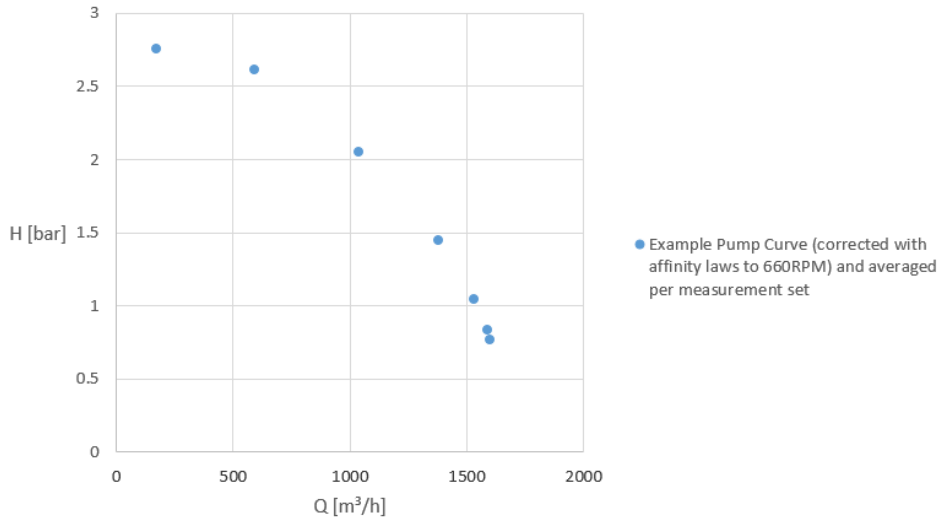

Figure 5.6: Pump Curve Example Averaged Per Measurement Set

Figure 5.6 shows the average point per measurement point from figure 5.5 (blue data points). Per measurement point at least 120 data points are available. As can be seen in 5.5, the 120 data points for every measurement are quite concentrated so an average over the 120 data points can be taken without any problem. These data points are then manually implemented in the *MATLAB*-files from chapter 6, to make it easier to work with. Everything just mentioned can be seen in every figure used further in this thesis.

6

WEAR PREDICTION

6.1. AXIAL GAP

6.1.1. PREVIOUS RESEARCH & WORK DONE

The data used for the axial gap was available due to previous research [1] on designing a process status evaluating tool. During this research, the sediment transport test circuit at Damen Dredging Equipment was used to perform four different tests to see the influence of only the axial gap on the pump behaviour. First the normal impeller and wear plates where inserted ($2mm$ gap), after that the gap was increased by repeating machining with $3mm$, until $11mm$ is reached. During the test the efficiency (η) and head (H) per flow rate (Q) were measured.

6.1.2. DEFINITION

The axial gap is the space between the impeller and the pump casing as can be seen in fig. 6.1. Two different gaps can be seen in this figure: one at the suction side (gap F) and another at the pressure side (gap E). These gaps are necessary for mechanical reasons. Only gap F is considered for the rest of this thesis, since there is no leakage from gap E to the impeller inlet and hence the effect on the pump performance is negligible.

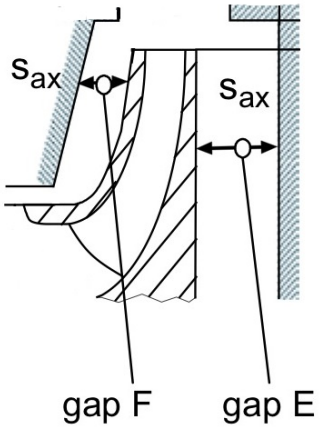

Figure 6.1: The axial gap [6]

FLOW PHENOMENA AND THEIR INFLUENCE

A centrifugal pump creates two types of vortices in the axial gap. The primary vortex is created by rotating the impeller and thus fluid inside the pump (fig. 6.2). While the secondary vortex is created due to the difference in rotation velocity between the fluid at the impeller surfaces and the pump casing, see fig. 6.3, these vortices are explained more in depth below [3].

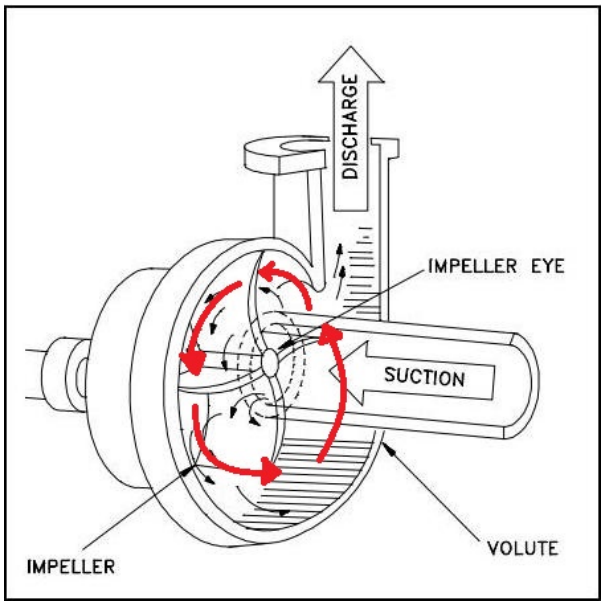

Figure 6.2: Primary vortex in the axial gap, red arrows indicate the vortex motion [7]

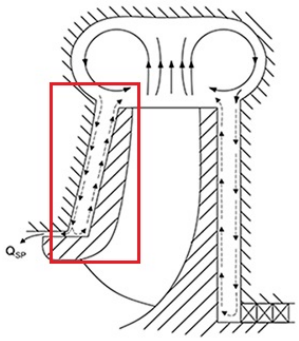

Figure 6.3: Secondary vortex and flowlines in the axial gap (inside the red rectangle) [6]

PRIMARY VORTEX

For the primary vortex (created by rotating the impeller) it is stated in Gülich[14], that when gap F is small ($s_{ax} < \delta$ with δ is equal to the boundary layer thickness) the velocity distribution in the axial gap is linear and the mean velocity is approximately $\frac{1}{2} \cdot \omega \cdot R$. When increasing the axial gap, the friction loss drops to a minimum due to a laminar flow in the axial gap. This has no practical significance since it cannot be executed in reality. For this thesis, the flow in the axial gap is assumed to be turbulent.

SECONDARY VORTEX

The fluid, very close to the suction shroud (also referred to as 'disk'), starts to move outward as a consequence of the centrifugal forces on the impeller. This creates a motion in the axial gap, a circulation. This phenomenon is called the secondary vortex. The secondary vortex transfers energy from the impeller to the wear plate and therefore increases the disk friction [3]. This energy transfer is delivered via the velocity difference between the two boundary layers present in the axial gap. The fluid adhered to the wear plate has no velocity ($C_u = 0$), while the fluid adhered to the impeller accelerates to $C_u = \omega \cdot R$. The velocity drops while the distance from the impeller increases. The circulating flow can be superimposed due to seal leakages (Q_{SP} in fig. 6.3, Q_L is further used from now on). A leakage is virtually always present on the suction shroud of the impeller, it carries a momentum into the impeller gap. This momentum enhances or retards the fluid rotation.

6.1.3. DISK FRICTION

Disk friction can be defined as the increased power consumption which occurs on the impeller surface because it rotates in a fluid-filled pump casing, therefore it affects the η. The amount of disk friction depends

primarily on the impeller speed & diameter, as well as the dimensions of the pump housing (in particular the axial gap) [3, 14].

The fundamental equation for disk friction is given by equation 6.1[15]. In this equation $(hp)_d$ is the power absorbed by disk friction, K is an experimental factor which also takes care of the units used, n is the revolutions per minute and D_2 is the disk outer diameter.

$$(hp)_d = Kn^3 D_2^5 \tag{6.1}$$

$$M = C_M \rho \omega^2 R_2^5 \tag{6.2}$$

The momentum equation is given by 6.2[16]: M is the moment (torque), C_M is the moment coefficient and R_2 the outer radius of the disk. Since the disk friction torque increases with the fifth power of the diameter, small changes in the diameter have a disproportionately large effect on the disk friction torque [6].

6.1.4. NON-DIMENSIONAL TORQUE COEFFICIENT C_M

Equation 6.2 shows the non-dimensional torque coefficient C_M [17]. This empirical coefficient shown in equation 6.3, is adapted with the following values for the coefficients: $A = -0.2$ assuming a turbulent regime, $B = 0.1$, $C = 0.25$ and $D = 0.2$ according to Nemdili [17].

$$C_M = \left(\frac{k_s}{R_2}\right)^C \cdot \left(\frac{s}{R_2}\right)^B \cdot \left(\frac{b_2}{s}\right)^D \cdot Re^A \tag{6.3}$$

In this equation k_s is the surface roughness coefficient, R_2 the outer radius of the impeller, b_2 the impeller outer width, s the axial gap width and Re the Reynolds number.

6.1.5. LEAKAGE

The leakage flow Q_L is defined as the momentum that flows from the axial gap back into the suction eye. The flow rate through the impeller, Q_{imp}, is equal to the sum of the measured flow rate (Q) and the leakage flow (Q_L), as can be seen in fig. 6.4.

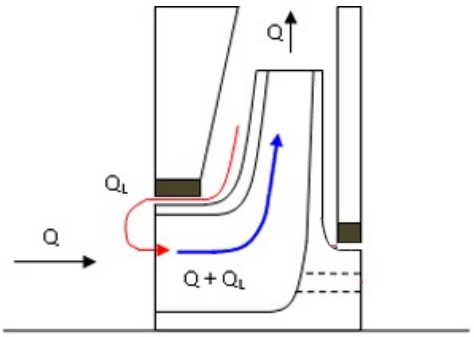

Figure 6.4: Leakage flow example [8]

Rewriting this sum results in eq. (6.4). From this it can be seen that the higher the leakage flow Q_L, the lower the measured flow rate will be Q. The produced head will stay the same because Q_{imp} remains the same section 1.1.4. This implies that the head-curve will have the same shape, but is shifted slightly towards the left.

$$Q = Q_{imp} - Q_L \tag{6.4}$$

6.1.6. DATA COMPARISON

Comparing the data for head (fig. 6.5) and $\eta_{Measured}$ (fig. 6.6), it can be seen that the most effect of the disk friction and especially the leakage can be seen in the $\eta_{Measured}$ data.

HEAD

For the head (fig. 6.5), the difference is the biggest at the right hand side of the BEP. The larger the axial gap becomes, the more the head curve is shifted to the left. This same difference can be seen at the left hand side of the BEP but way smaller. This phenomenon is mentioned and explained in section 6.1.5. It was expected that the head curve would shift to the left, but not that it would decrease this much on the right hand side of the BEP. An explanation is not yet available for this larger decrease.

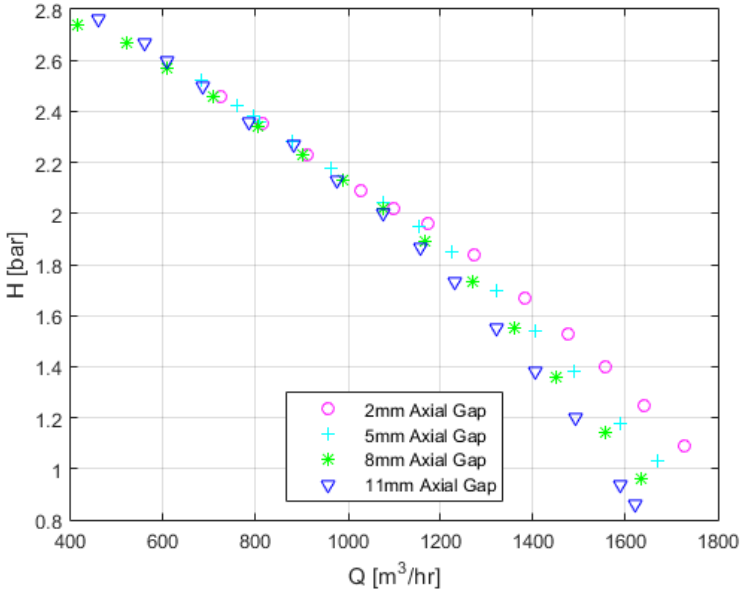

Figure 6.5: Head comparison between different axial gap distances [1]

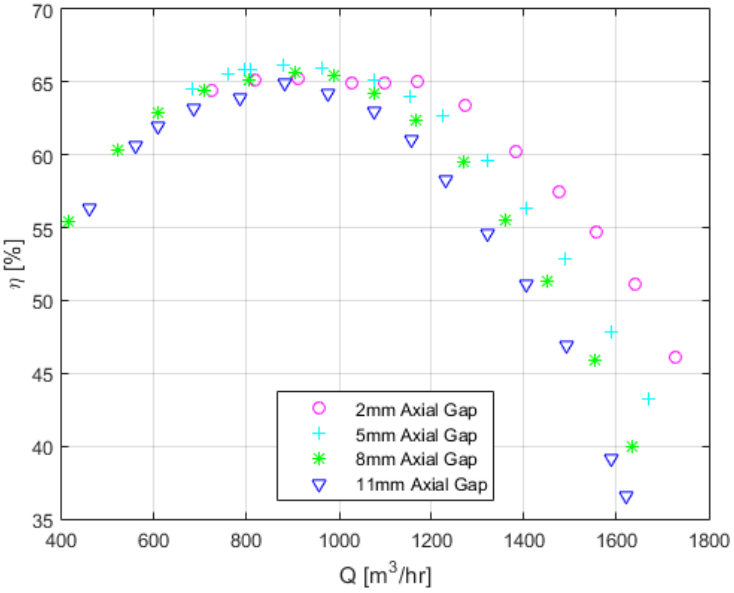

Figure 6.6: Efficiency comparison between different axial gap distances [1]

$\eta_{Measured}$

eq. (6.6) shows the two most important parameters to explain the difference in $\eta_{Measured}$ (fig. 6.6), $\triangle p_{tot}$ & Q. $\triangle p_{tot}$ is defined as the pressure difference between the exit and entrance of the pump. The differences mentioned in 6.1.6 can be seen in figure 6.6. Looking at the BEP, it can be seen that it is shifted to the left,

and that there is a small decrease in maximum value, see 6.11. And the big difference right from the *BEP* is the difference as discussed in section 6.1.6 (*head*). Equation 6.6 is obtained by substituting eq. (1.17) into eq. (6.5).

$$\eta_{Measured} = \frac{P_{hydr}}{P_{shaft}} \tag{6.5}$$

$$\eta_{Measured} = \frac{\triangle p_{tot} Q}{P_{shaft}} \tag{6.6}$$

6.1.7. MODEL

In this section, the equations that were used for the model are explained. Making a model always implies making assumptions, these assumption introduce small errors and problems. To match the model to the results (to include errors), an own empirical coefficient is introduced.

EQUATIONS

H_{DF} is the head loss due to disk friction and is equal to the disk friction power divided by the flow rate, as can be seen from equation 6.7. All the other variables are already discussed earlier on in section 6.1.3 & section 6.1.5.

$$H_{DF} = \frac{C_m \cdot \rho \cdot \omega^3 (D/2)^5}{Q} \tag{6.7}$$

Equation 6.8 describes the volumetric flow rate loss Q_L. This is a simple orifice equation: the cross-sectional area of the flow is multiplied by a contraction coefficient C_{Q_L} and also multiplied by the difference between the theoretical head $H_{Theoretical}$ (eq. (1.22)) and a quarter of the velocity head of the tangential velocity $\frac{1}{4} \cdot \frac{U_2^2}{2g}$ according to Nemdili [17].

$$Q_L = C_{Q_L} \cdot s \cdot \pi \cdot D_2 \cdot \left(H_{Theoretical} - \frac{{U_2}^2}{8g} \right) \tag{6.8}$$

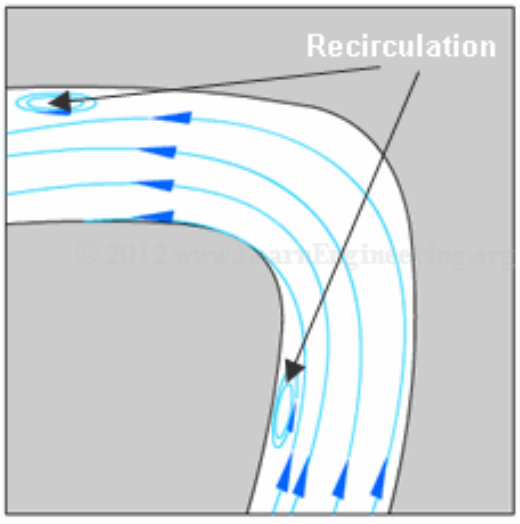

Figure 6.7: Example of recirculation in a flow [9]

To be able to calculate the efficiency [6], eq. (6.10) , it was assumed that the recirculation head $H_{recirculation}$ is equal to zero. This means that it is assumed that there are no recirculation present in the flow. Also the pump head $H_{measured}$ is not calculated, but used from the experiments. Doing this it was able to compare and validate the calculated efficiency and the measured efficiency with respect to the same pump head.

$$H_{recirculation} = 0 \tag{6.9}$$

$$\eta_{model} = 100 \cdot \frac{H_{measured}}{H_{Theoretical} + H_{DF} + H_{recirculation}} \cdot \frac{Q}{Q + Q_L} \tag{6.10}$$

6.1.8. EFFICIENCY COMPARISON BETWEEN ($\eta_{Measured}$) AND (η_{model})

Looking at fig. 6.8, a large difference between the measured efficiency ($\eta_{Measured}$) and the calculated efficiency (η_{model}) can be distinguished. In an ideal situation there would be no difference between the two situations. After looking more closer into η_{model}, a decreasing linear relationship can be observed between the Best Efficiency Points (BEP). This difference is eliminated by an empirical coefficient that will be multiplied with η_{model} (equation 6.11). Before the empirical coefficient was added, a deeper look into the possible cause of this large difference between η_{model} and $\eta_{Measured}$. A possible cause is $H_{theoretical}$, so the exact influence was investigated. Multiplying $H_{theoretical}$ with a certain loss factor of 0.6 gives the same result as $\eta_{model} \cdot 2$ (fig. 6.9). Therefore C_{MDB} is going to be used, since this will eliminate also the other differences as explained in section 6.1.9.

6.1.9. EMPIRICAL COEFFICIENT C_{MDB}

Equation 6.11 for the coefficient C_{MDB}, shows an empirical relationship with the axial gap (s) as variable. First the difference between the maximum efficiency of $\eta_{model2mm}$ and $\eta_{Measured2mm}$ is made zero by multiplying a factor 2. This is seen in the left part of the right hand side of equation 6.11. This effect is shown in figure 6.9.

For an increasing axial gap, the difference between $\eta_{Measured}$ and $(\eta_{model} \cdot 2)$ is linearly increasing. To match every η_{model} with its corresponding $\eta_{Measured}$, a factor of $(0.76/0.003) \cdot (s - 0.002)$ was used to match this difference. This factor is found after a trail-and-error method. The differences are not exact zero because the difference is not exact linear, so a more exact model can be developed in a future research. In every figure, s is shown in mm but has to be implemented in eq. (6.11) in m.

$$C_{MDB} = 2 + (0.76/0.003) \cdot (s - 0.002) \tag{6.11}$$

Tis equation (6.11) is multiplied with 6.10, to get a new η_{model} resulting in eq. (6.13). This can be seen in fig. 6.10. From this moment on, this new η_{model} will be used.

$$\eta_{model1} = C_{MDB} \cdot \eta_{model} \tag{6.12}$$

$$\eta_{model1} = C_{MDB} \cdot 100 \cdot \frac{H_{measured}}{H_{Theoretical} + H_{DF} + H_{recirculation}} \cdot \frac{Q}{Q + Q_L} \tag{6.13}$$

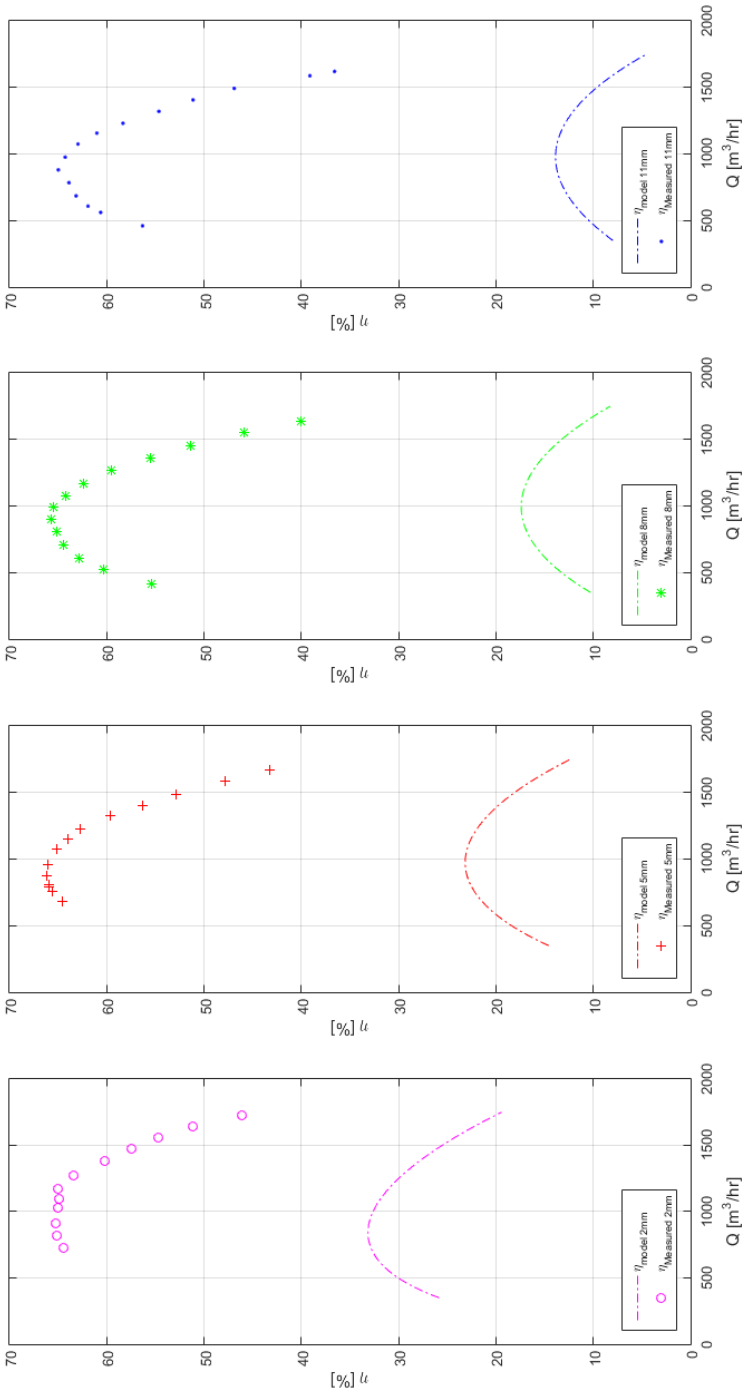

Figure 6.8: Efficiency comparison between $\eta_{Measured}$ and η_{model} [1]

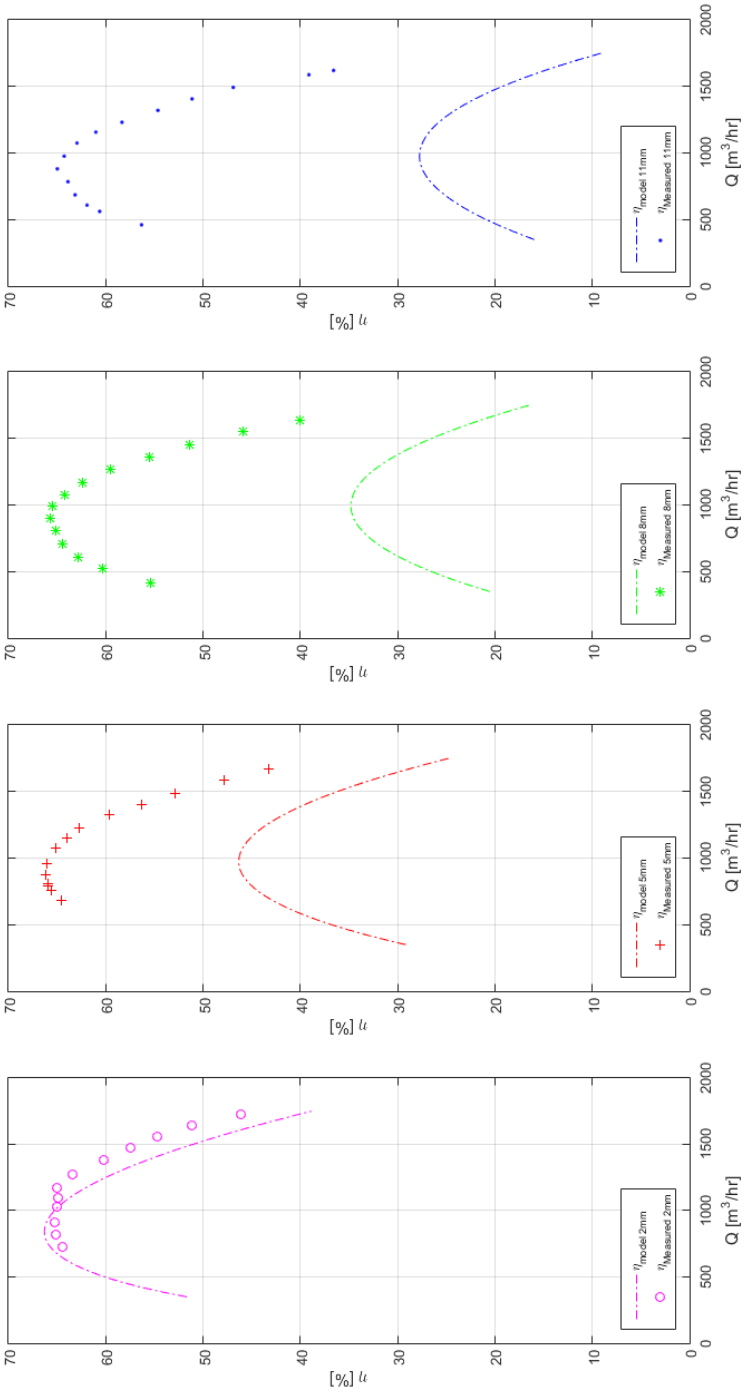

Figure 6.9: Efficiency comparison between $\eta_{Measured}$ and $\eta_{model} \cdot 2$ [1]

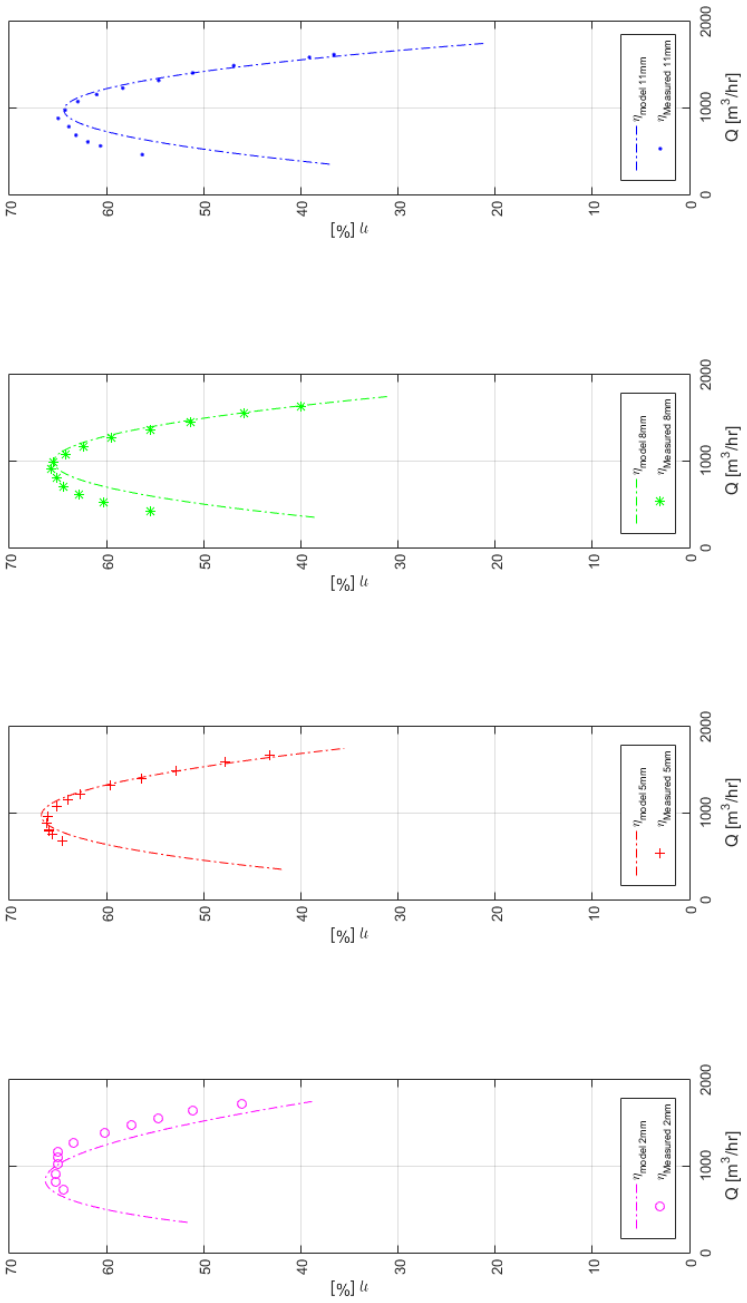

Figure 6.10: Efficiency comparison between ($\eta_{Measured}$) and (η_{model1}) [1]

6.1.10. HOW TO CALCULATE THE AXIAL GAP s FROM MEASURED PARAMETERS?

Figure 6.10 shows the BEP of both η_{model} and $\eta_{Measured}$ with the axial gap s as variable. To plot the BEP of η_{model}, s was assumed to be known. Looking at fig. 6.10 it can be seen that if s is known, the difference between the value for BEP of η_{model} and $\eta_{Measured}$ is minimal. No exact relationship between the BEP of η_{model} and the axial gap s can be found since the differences are small and not consistent.

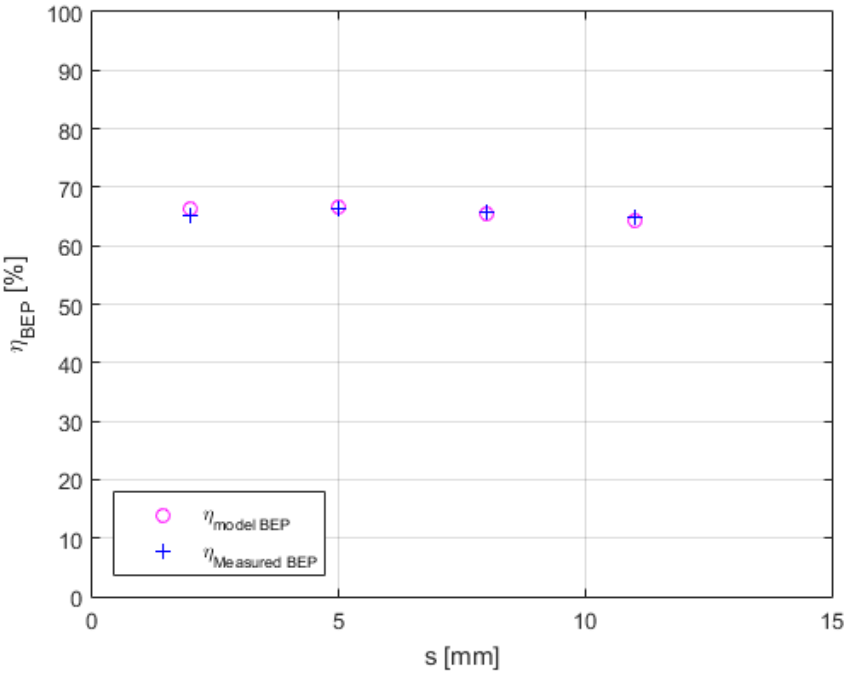

Figure 6.11: Comparison of η_{model} with $\eta_{Measured}$ in function of the axial gap s

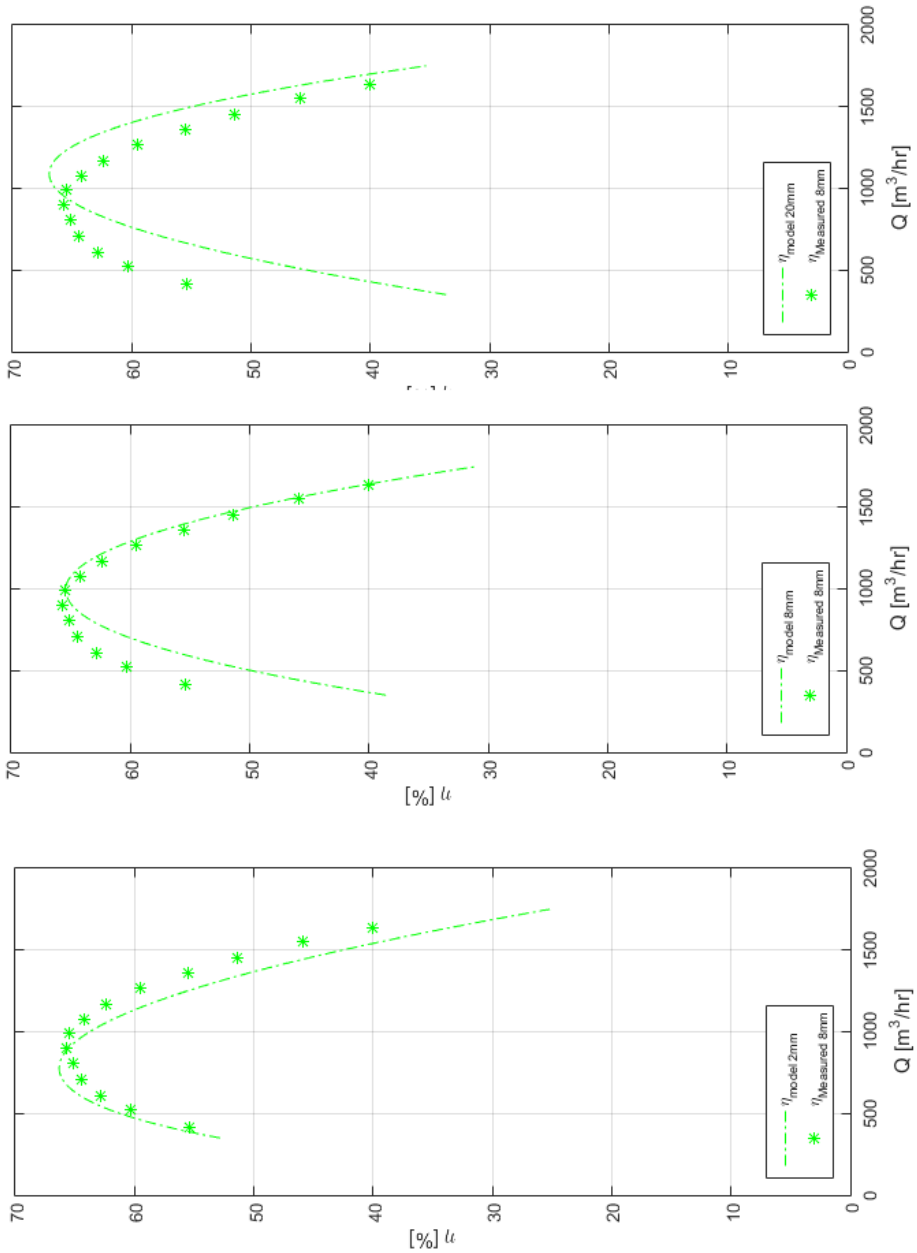

Figure 6.12: Comparison of η_{model} with $\eta_{Measured}$ in function of the axial gap s for an axial gap width of $2mm$, $8mm$ and $20mm$

Another method to estimate the axial gap s is by guessing s and use this in eq. (6.13) to see if η_{model} converges with $\eta_{Measured}$. An example of this trial-and-error method is seen in fig. 6.12. This figure shows the extrema (s is equal to $2mm$, $8mm$ and $20mm$) of the trail-and-error method for $\eta_{Measured8mm}$, which is fully shown in appendix B. The other figures in appendix B shows $\eta_{Measured}$ for an axial gap width of: $2mm$, $5mm$, $8mm$ and $11mm$. For every $\eta_{Measured}$, different axial gap dimensions were used to see when η_{model} converges with $\eta_{Measured}$. The dimensions used are: $2mm$, $5mm$, $8mm$, $11mm$, $14mm$, $17mm$ and $20mm$. Figure 6.12 shows three different axial gap widths ($2mm$, $8mm$ and $20mm$) that were used to estimate the axial gap width s. The conclusions that can be drawn from this trial-and-error method from appendix B, can also be seen in fig. 6.12. The conclusions are as follows:

- When the right part of η_{model} is left from the data points from $\eta_{Measured}$, the axial gap width used is too small.
- When the right part of η_{model} is right from the data points from $\eta_{Measured}$, the axial gap width used is too high.

- When the right part of η_{model} converges with the data points from $\eta_{Measured}$, the axial gap width used is (approximately) correct.
- An exact solution for the axial gap width (s) can not be found since there are some errors present e.g. measurement errors. The difference between small axial gap variations is difficult to predict, but an estimation whether the axial gap is small or large can be made.

6.2. INNER DIAMETER CHANGE IMPELLER

In this section the influence of the inner diameter change of the impeller on the pump parameters is investigated and discussed. The considered parameter are the $Q-H$ curve, efficiency (η) and the $NPSH_{3\%}$ ($NPSH_R$). These are discussed in the same order as mentioned. The inner diameter is increased in 3 steps, first an increase of $6mm$ is machined, second $18mm$ and last $48mm$. These increases are the total inner diameter increase, not increase per step.

6.2.1. $Q-H$ CURVE

The $Q-H$ curve is the easiest way of getting information out of the system, it does not need a lot of testing time nor data processing.

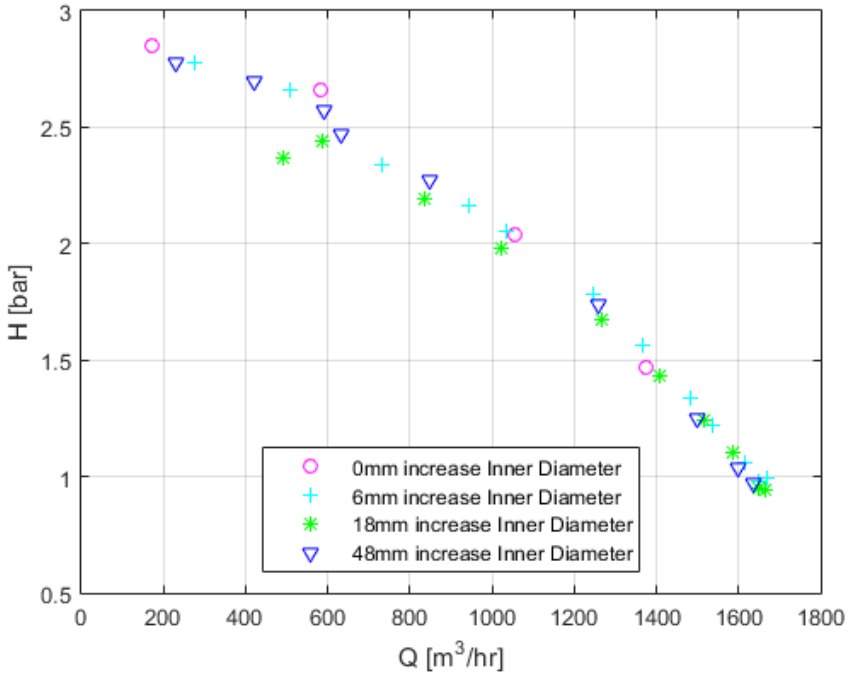

Figure 6.13: Combined head curves test 1.1.1, 1.2.1, 1.3.1 and 1.4.1

Figure 6.13 shows the different $Q-H$ curves for increasing inner diameter. A decreasing trend can be seen excluding the $48mm$ inner diameter increase. This head increase is explained after the elaboration of the decreasing trend for the other test data in section 6.2.1. Another general trend is the horizontal position of the last point of the $Q-H$ curve (seen from right to left). A larger inner diameter means a shift towards right for the last point. This is caused by instability of the flow at the suction entrance and blade entrances, the flow starts to cavitate at smaller flows.

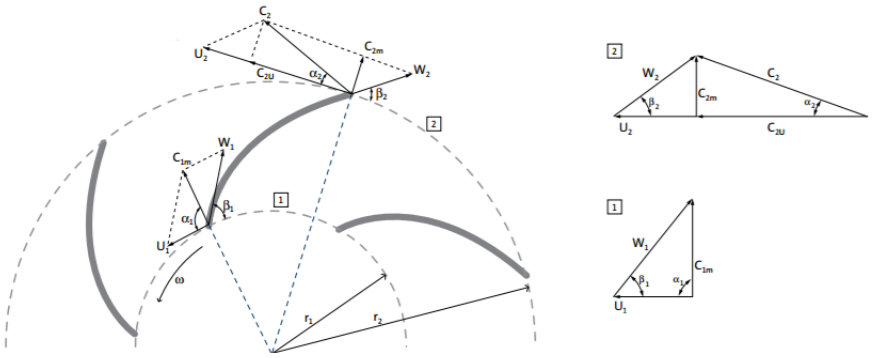

Figure 6.14: Velocity triangles positioned at the impeller inlet and outlet [3]

To be able to find a relationship between the effects of the different inner diameters and their corresponding generated head, the main question is: How is head generated in a centrifugal pump? Figure 6.14 shows the velocity vectors in a centrifugal pump with their according velocity triangles. This phenomenon is already explained and elaborated in chapter 1.

From the velocity triangles (explained in section 1.1.4, the Euler's pump equation, eq. (6.14) is found. This is the same equation (eq. (1.22)) found in chapter 1 but repeated here for simplicity. This equations consists of 3 parts which each generate head: static head as consequence of the centrifugal force, the static head as consequence of the velocity change through the impeller and the dynamic head.

$$H = \frac{U_2^2 - U_1^2}{2g} + \frac{W_1^2 - W_2^2}{2g} + \frac{C_2^2 - C_1^2}{2g} \tag{6.14}$$

VERTICAL SHIFT OF HEAD

By studying eq. (6.14), the vertical shift can be explained by the static head generated by the centrifugal force. The centrifugal velocity at the inlet (U_1) increases, resulting in a decrease of the total head. For simplicity, only the static head generation is looked after: $H = \frac{U_2^2 - U_1^2}{2g}$ With: $U_{1,2} = 2\pi r_{1,2} \frac{n}{60}$. Combining these two equations results in eq. (6.15). So when elaborating the affinity laws, and hence including the effect of the inner diameter, results in equation 6.15.

$$\frac{H_{D_{in,2}}}{H_{D_{in,1}}} = \left(\frac{n_2}{n_1}\right)^2 \frac{D_{out,2}^2 - D_{in,2}^2}{D_{out,1}^2 - D_{in,1}^2} \tag{6.15}$$

Inner Diameter	$H_{measured@BEP}$	$H_{equation1,@BEP}$ with eq. (6.15)	**Error Rate equation 1 (eq. (6.15))** [%]	$H_{equation2,@BEP}$	**Error Rate equation 2 (eq. (6.16))** [%]
0mm increase	2.3	/	/	/	/
6mm increase	2.22	2.28	2.7	2.23	0.5
18mm increase	2.13	2.23	4.6	2.08	2.3
48mm increase	2.32	2.11	9.9	1.74	25

The results from equation 6.15 are within a 5% accuracy rate which is quite accurate. The values used for the head is the head at the BEP. Every value and error rate are shown in section 6.2.1.

Another approach comes from the original affinity law (equation 6.16) and considering an effective diameter which is equal to: $D_{eff} = D_{out} - D_{in}$. This effective diameter is considered to be the total distance the fluid has to accelerate. This method has a maximum error rate of 2.3% which is half of the error rate of the other method, all the error rates are shown in section 6.2.1. This approach cannot be explained yet, to make sure it is not a lucky guess, more and different pumps have to be tested. After this, a conclusion can be drawn if this approach is a coincidence or not.

$$\frac{H_2}{H_1} = \left(\frac{n_2}{n_1}\right)^2 \frac{D_{eff,2}^2}{D_{eff,1}^2} \tag{6.16}$$

48 MM INNER DIAMETER HEAD INCREASE

The increase of head of the $48mm$ inner diameter increase (fig. 6.13, was not expected to happen. There is not yet an explanation of the exact reason why this happened. Only decrease of head was expected, the inlet angle increases (from 38° to 65°), so according to section 1.1.4, the head would decrease, and another head decrease is explained with eq. (6.15).

6.2.2. EFFICIENCY

The BEP is used to compare the different curves with each other, and is also used for the $Q-H$ curve. In general, there is no consistency comparing the BEP from the different tests. A small increase of the inner diameter gives an increase of the maximum η, while a larger increase results in a decrease of the maximum η, while the largest increase result again in an increase of the maximum η. The scattering of the different data is minimal, and therefore difficult to find a relationship. Therefore the focus is on the $Q-H$ curve.

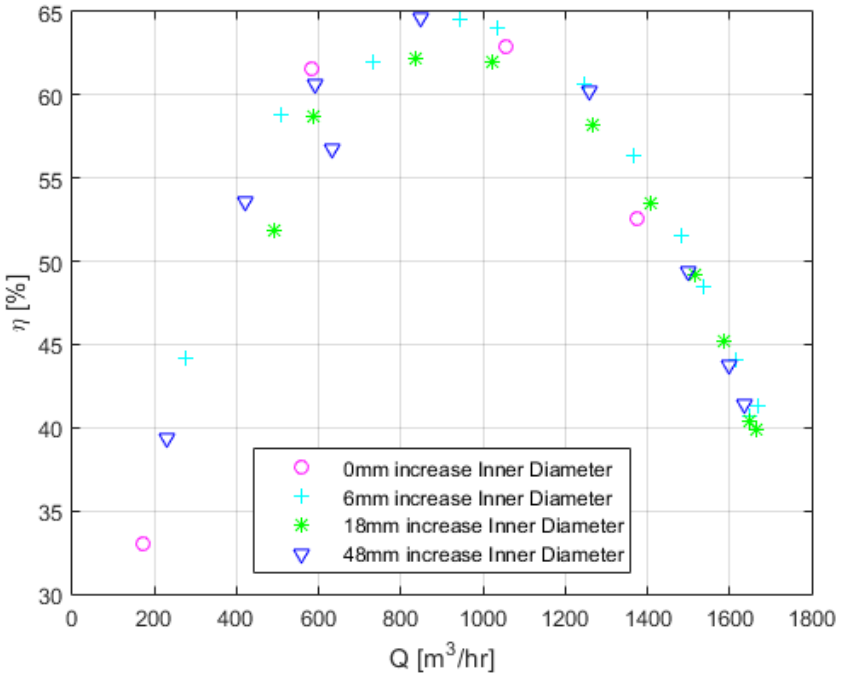

Figure 6.15: Combined efficiency curves test 1.1.1, 1.2.1, 1.3.1 and 1.4.1

6.2.3. $NPSH_{3\%}$

The net positive suction head required ($NPSH_R$) is the minimal head required to keep the fluid, in the suction entrance, from cavitating. It is also called the $NPSH_{3\%}$ due to the fact that a 3% reduction of the head is used to determine the $NPSH_R$. The work method used to determine the $NPSH_{3\%}$ is based on the one in Grundfos [3]: gradually lower the inlet pressure while while the flow is kept constant, this method can be seen in fig. 6.16. The red box indicates one measurement set (Measured head in fig. 6.16), in fig. 6.17 till fig. 6.20 referred to as 'measured head' with the measurement set number. The orange box is the corresponding $NPSH_A$ for the red box measurement set. The number of measurement sets made in the own experiments (fig. 6.17 till fig. 6.20) are at least 3 with at least 5 measurement points per measurement set, as defined in section 5.5.2. Fig. 6.16 also shows a reference Q-H curve together with its 3% reduction curve. The orange crosses in fig. 6.16 are the $NPSH_A$ calculated by implementing the measured head (measurement sets) in eq. (6.17). The $NPSH_{3\%}$ curve can be determined from the $NPSH_A$ measurement points. The exact data point from the $NPSH_A$ that is chosen depends on its corresponding measured head (red crosses). The

last point before the measured head reaches the 3% curve (in fig. 6.16) is the data point needed. For example for the most right measurement set in fig. 6.16, the third point (counting from top to bottom) is the last point from this measurement set before reaching the 3% curve. Therefore the third point from the $NPSH_A$ is a reference point for the $NPSH_{3\%}$ curve [3].

$$NPSH_A = P_s + \frac{1}{2}\rho V^2 + h_s(\rho g) - P_{vap} \tag{6.17}$$

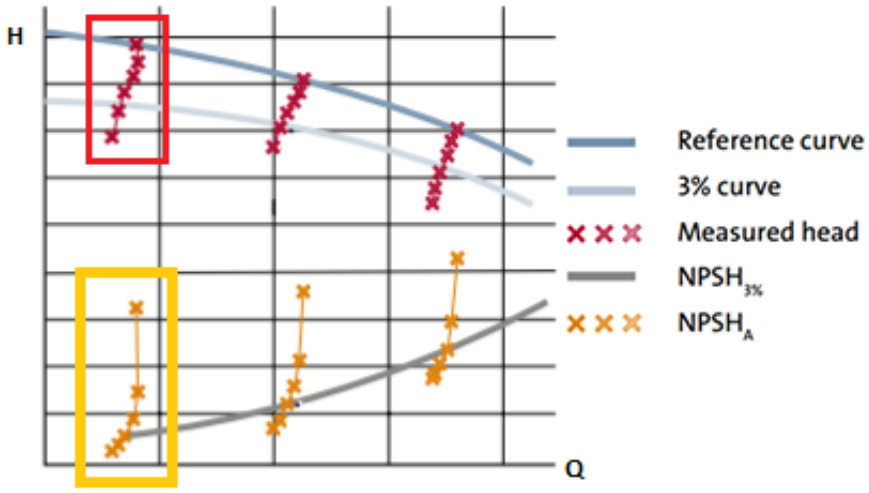

Figure 6.16: Determination of $NPSH_{3\%}$ [3]

WORK METHOD MEASURED HEAD TESTS

The way the sediment transport circuit is used is defined in section 5.3.2, the exact work method for every measurement set is described in this section. First a Q-H test is made which is used as a reference curve from which the 3% head reduction curve is made. After this at least 3 measurement sets are made. One measurement set is made as follows: the flow rate is chosen using DGV2 (different for every measurement set, the position of DGV2 determines the flow rate), after this the pressure at the entrance has to be lowered gradually (until the 3% head reduction is reached) by closing DGV5 in small steps (5 at least). The pressure at the entrance of the pump is lowered because less water has the possibility to get pumped through the pump (based on the principle of creating a vacuum). The next measurement set is than created by choosing another valve setting for the DGV2 and repeating the other steps.

TEST RESULTS

The figures used in this subsection (fig. 6.17 till fig. 6.20) are results from own experiments. The technique discussed during previous subsections from section 6.2.3 is used to get to fig. 6.21. In these figures the upper part of fig. 6.16 can be seen and 'measured head 1' is the measurement set for a certain valve (DGV2) opening while 'measured head 2 & 3' are measurement sets for respectively two other valve (DGV2) settings.

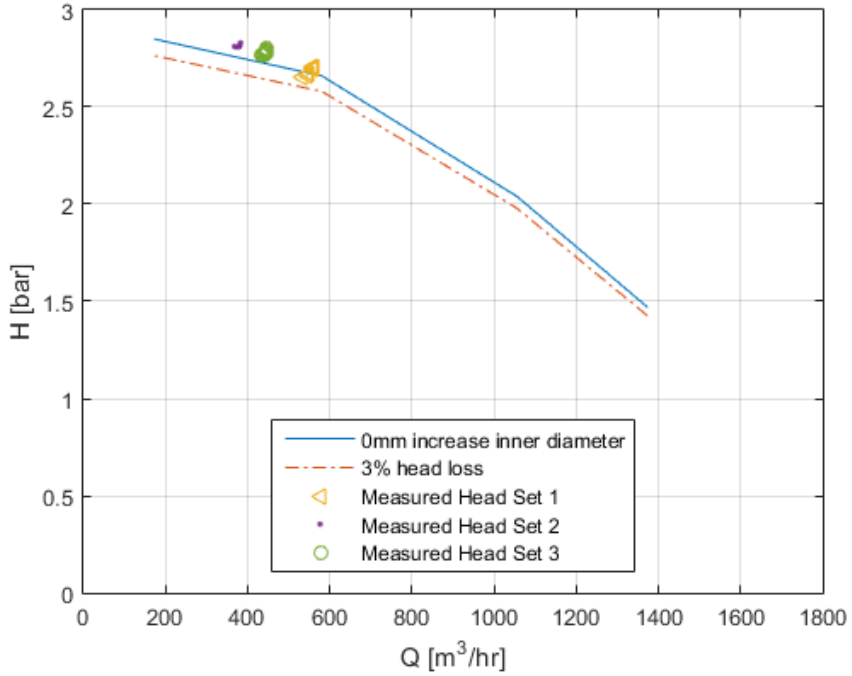

Figure 6.17: Measured head test 1.1.2

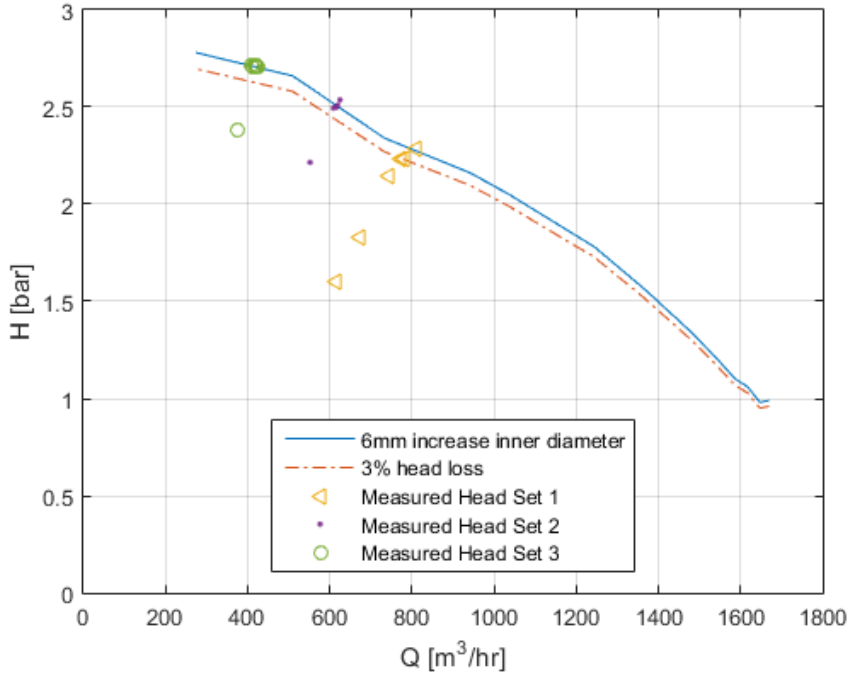

Figure 6.18: Measured head test 1.2.2

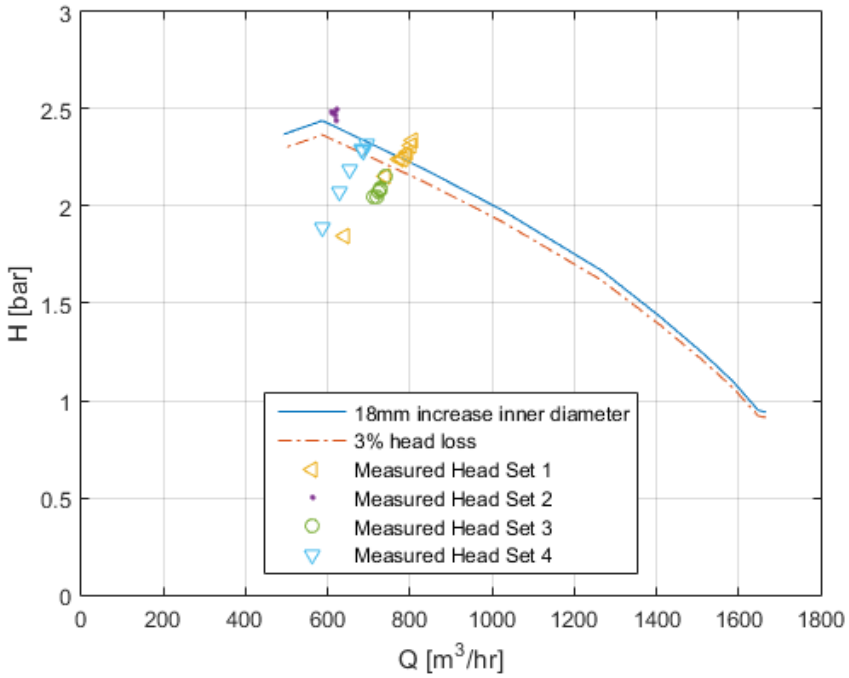

Figure 6.19: Measured head test 1.3.2

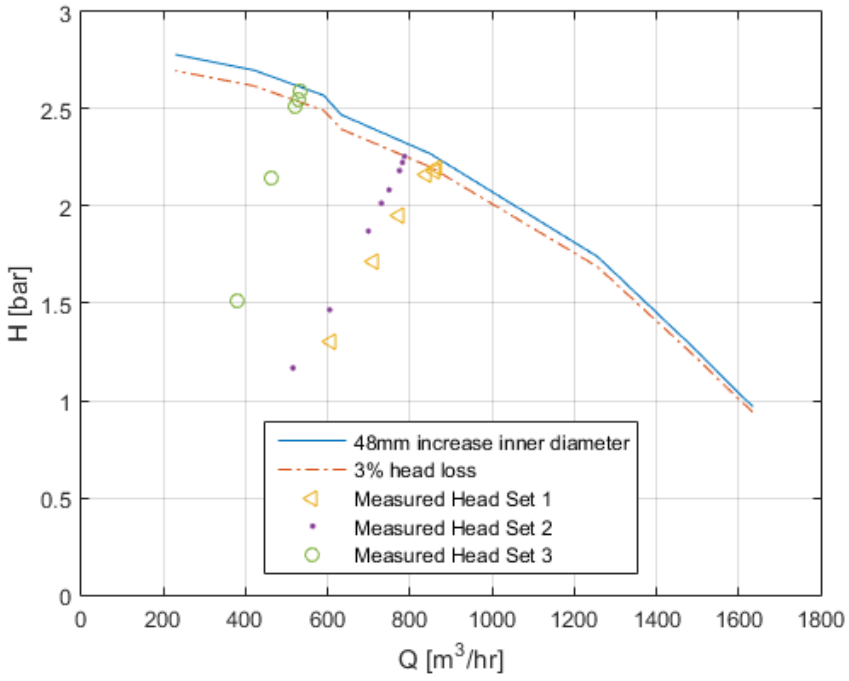

Figure 6.20: Measured head test 1.4.2

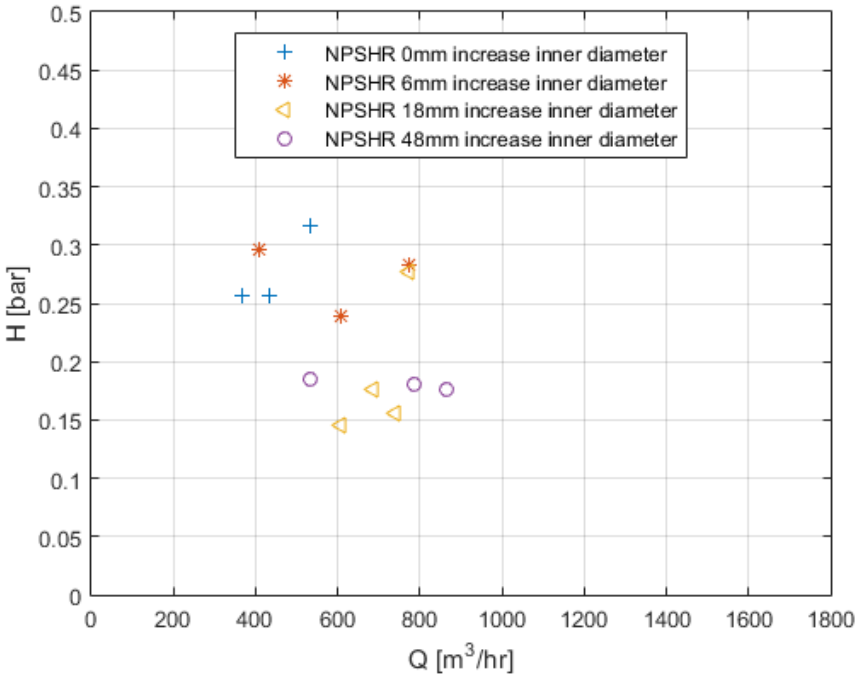

Figure 6.21: Calculated $NPSH_{3\%}$ from test 1.1.2, 1.2.2, 1.3.2 and 1.4.2

Figure 6.21 shows the $NPSH_{3\%}$ curve for every test (1.1.2, 1.2.2, 1.3.2 and 1.4.2). It is the result from applying fig. 6.16 to fig. 6.17 till fig. 6.20. As can be seen in figure 6.21 (combination of all test), the data points per test are too scattered to find a relationship between the various tests. The data is already adjusted for the small variation in temperature (to correct P_{vap}). When comparing the general tendency of every test with each other, a general decrease of the $NPSH_{3\%}$ is noticed. No general conclusion or relationship can be found. The system seemed to be too unstable to get usable results, so the $NPSH$ could not be measured decent. This instability can be explained by the use of an open system (section 5.3.2), due to the fact that the basin (hopper) is too small.

6.3. VIBRATION ANALYSIS

In the first subsection 6.3.1, the general tendency of the pump vibrations is discussed. After that, subsection 6.3.2 elaborates on the influence of wear on the pump behaviour. Only the influence of wear on the vibration is shown in this section. For further research the influence of following things should be investigated: the misalignment of the impeller, a missing blade, different slurry type, and wear of individual components of the impeller.

6.3.1. NEW PUMP & WEAR PARTS

As can be seen in fig. 6.22 and fig. 6.23, the flow is stable for every flow rate Q (data points can be measured until almost zero flow rate).

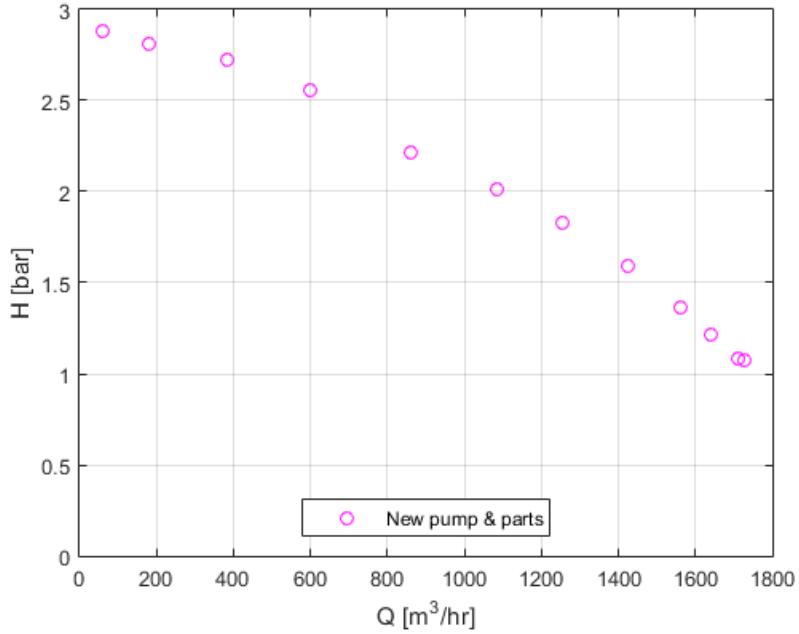

Figure 6.22: Head Curve New Pump & Wear Parts, test 2.1.1

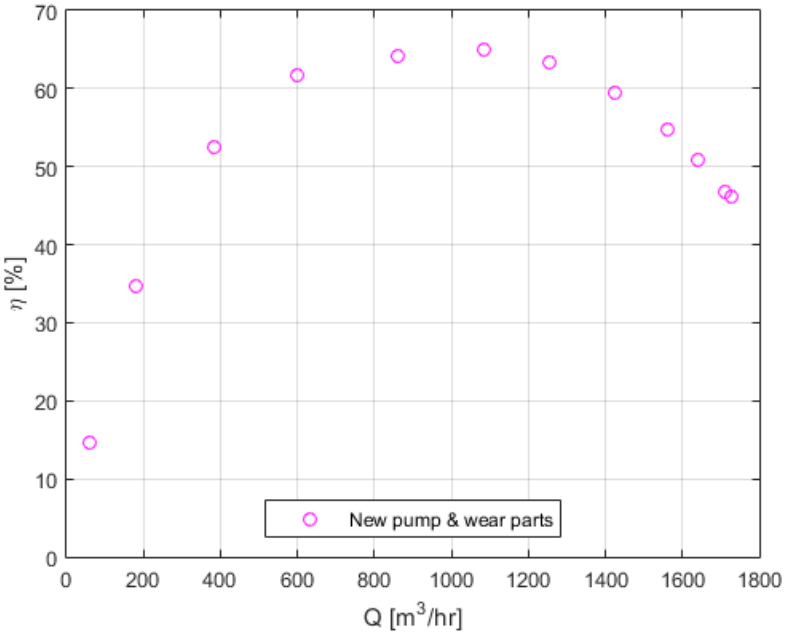

Figure 6.23: Efficiency Curve New Pump & Wear Parts, test 2.1.1

In fig. 6.24 and fig. 6.28, three directions are shown. The tangential (or X-direction), the radial (or Y-direction) and the axial (or Z-direction). This can be seen in fig. 6.25, only the Z-axis is not visible because it is directed outwards from the paper. The scattering of the data points, in every direction, is negligible.

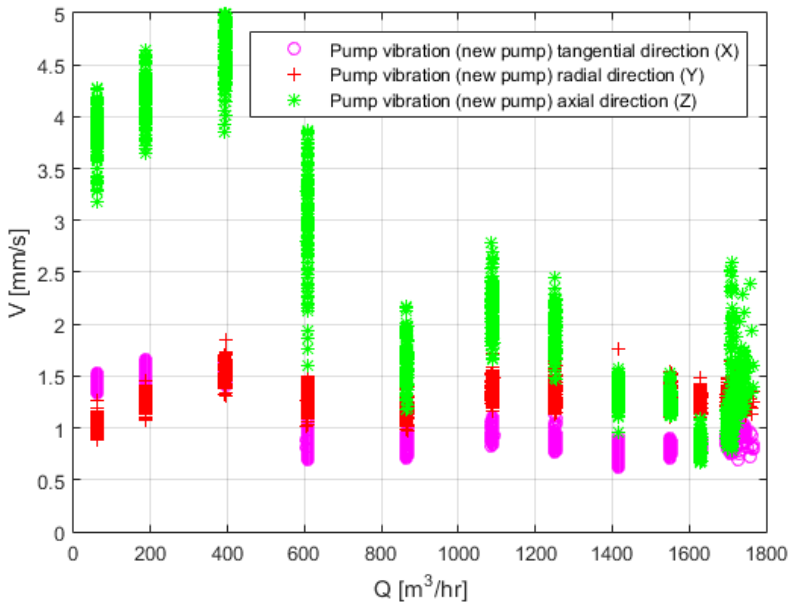

Figure 6.24: Vibration Curve New Pump & Wear Parts, test 2.1.1

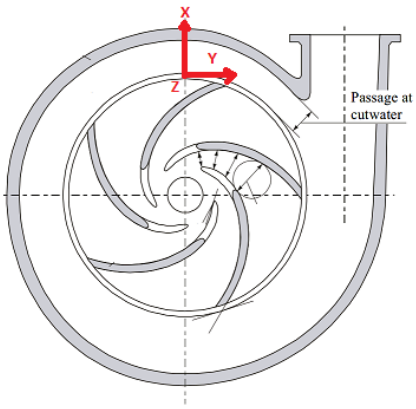

Figure 6.25: Vibration Sensor Placement and Axis Definition [1]

When comparing fig. 6.23 and fig. 6.24, it can be seen that when the flow rate Q approaches the BEP, the vibrational velocity will be lower. Left from the BEP, the axial vibrational velocity will rise very quickly.

6.3.2. WORN PUMP & WEAR PARTS

The main difference between fig. 6.22 & fig. 6.26 and fig. 6.23 & fig. 6.27 is the position of the last stable point measured (last point from right to left). Left from this point the flow became so unstable that it was not possible to gather data for the head H and efficiency η.

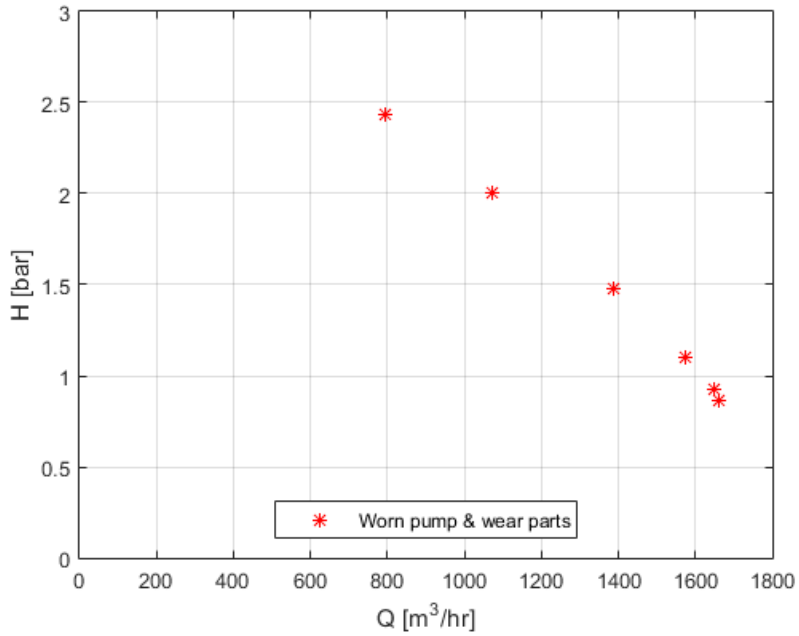

Figure 6.26: Head Curve Worn Pump & Wear Parts, test 2.2.1

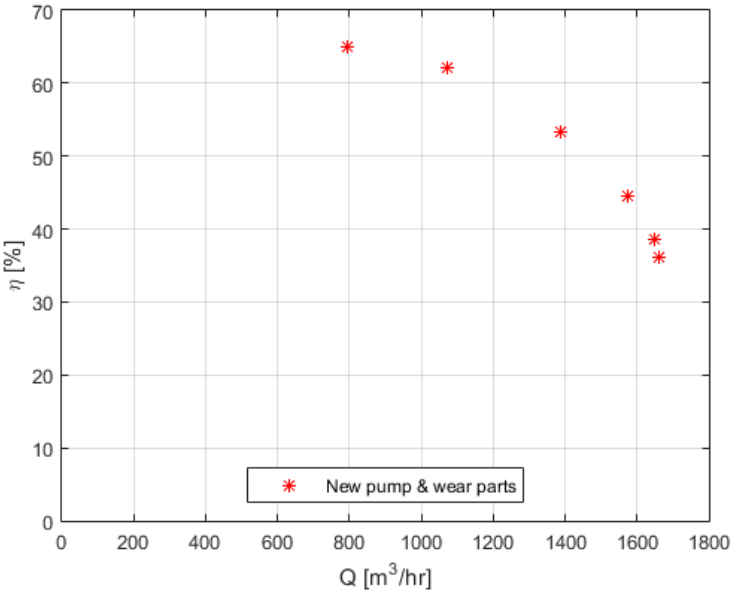

Figure 6.27: Efficiency Curve Worn Pump & Wear Parts, test 2.2.1

For fig. 6.28, the data left from the last stable point in fig. 6.26 and fig. 6.27 is shown. The data is very scattered, this indicates cavitation. The general tendency for the vibrational velocity in ever direction is that it decreases with increasing wear. A possible explanation for this phenomenon is that the outer tangential and radial velocity decreases, these lower velocities inside the pump could be visible in the vibrational velocities.

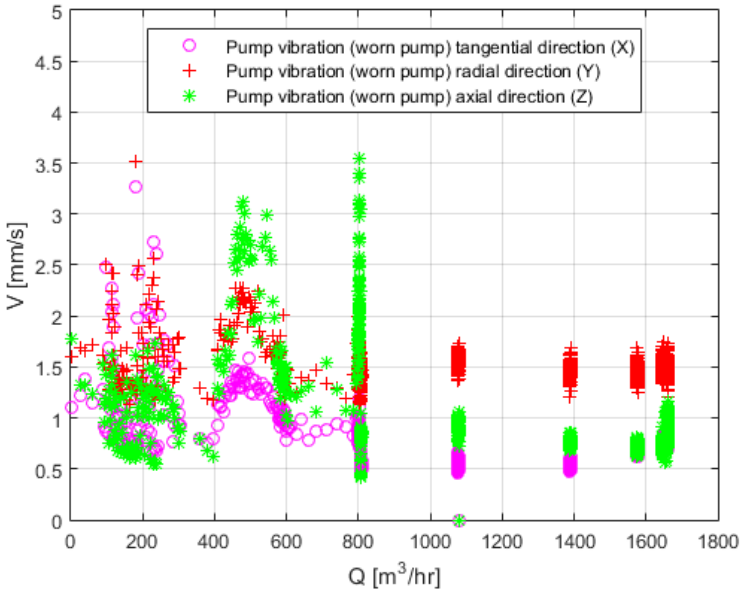

Figure 6.28: Vibration Curve Worn Pump & Wear Parts

The left part of fig. 6.28 shows a high scattering of all axes, while the right part shows no scattering at all (except at the highest flow rate a small scattering is visible). Therefore it is expected that the left part shows that the pump cavitates, this was also audible when operating the pump in the sediment transport circuit.

6.3.3. CONCLUSION VIBRATIONAL ANALYSIS

The BEP can be found through vibrational analysis, the vibrational velocity will be minimum here. Hence it can be used to monitor a displacement of the BEP due to wear. When a lot of scattering is seen in the data points, cavitation occurs in the pump. Therefore the vibration sensor can be used as a monitoring tool to warn the operator when cavitation occurs in the pump (so he can adjust the settings). A last thing that is seen from the vibrational analysis is when the working point is left from the BEP, high vibrations in the axial directions is observed.

7

CONCLUSION

This thesis is a part of the quest from Damen Dredging Equipment (DDE) to make their CSD (cutter suction dredger) or DOP pump operable by everyone for every slurry type at a correct working point every time. The first part in this quest is to design a "*Process Status Evaluation Tool*", which replaces the visual wear inspection. The first step to design such a tool is to understand the influence of wear on the wear plate and on every impeller dimension. The research question hence is "How can the pump process status be evaluated pumping water?"

In this thesis, first the possible wear locations are examined and the most important are chosen, hence the influence of the axial gap on suction side and the increase of the inner diameter is researched by looking at the change of the pump parameters (head H, efficiency η and Net Positive Suction Head $NPSH$). For this, different wear plate thickness (influence axial gap) and different sizes of inner diameter are tested in the sediment transport circuit at DDE (the axial gap data was available due to previous research [1] and the other data is available due to own experiments). Also another condition monitoring method is investigated (vibrational analysis), after first the different possible methods are discussed. For the influence of the axial gap and inner diameter, only the pump parameters are considered (vibration sensors were not available at that time). The vibration analysis is used to see if differences between the data of a new impeller & wear parts and worn impeller & wear parts could be detected. This impeller & wear parts are worn out in the sediment transport circuit at DDE by pumping a slurry (sand-water mixture) through the circuit.

During the research of the influence of the axial gap (section 6.1), it was found that it is possible to get an estimation of the axial gap width, this can be done by a 'trial-and-error' method. This is not an exact solution since the data for $2mm$ vs $5mm$ is almost the same, while a larger difference in axial gap width ($2mm$ vs $11mm$) can be easily seen in the data. The model cannot predict the exact axial gap width, but it can indicate whether or not the axial gap is small or large.
The influence of the inner diameter increase, the decrease of head at BEP, can be explained by the velocity triangles in section 1.1.3. Two different equations were found : one directly by using the velocity triangles resulting in eq. (6.15) and another one by using an effective diameter $\left(D_{eff} = D_{out} - D_{in}\right)$ into the affinity laws resulting in eq. (6.16). Equation 6.16 gives a better error rate in comparison with eq. (6.15) (5% for eq. (6.15) and 2.3% for eq. (6.16). To see whether or not eq. (6.16) is a lucky shot, more research should be done using more and different kinds of pumps. The $NPSH$ could not be measured decent so nothing could be concluded about that part.

The vibrations were measured in three directions: radial (X-axis), tangential (Y-axis) and axial (Z-axis). The vibration analysis clearly indicates: when the pump reaches it BEP (decrease of overal vibrations), when the pump cavitates (scattering of data points is high) and when the working point is left of the BEP (high axial vibrations).

Some possible future research:

- Check whether or not eq. (6.16) is a lucky guess or not. This can be done by testing more and different types of pumps.

- Combine findings for changes of axial gap, inner diameter and the known effect for outer diameter. Test combinations of these changes and compare it to the results found in this thesis and the already known affinity laws.
- Use different impellers for vibrational analysis: worn in real life, imbalanced, missing piece in one blade. Also test the impact on vibration for changing wear part & impeller dimensions.
- Test influence of other changing impeller dimensions on pump parameters and vibrations, see chapter 3 for other possible dimensions.

A

DOP250 Specifications

DAMEN

DOP 250

SUBMERSIBLE DREDGE PUMP

A hydraulically driven, submersible dredge pump with wear resistant pump parts. The construction details are as follows.

Dimensions	: Suction diameter	:	250 mm
	Discharge connection diameter	:	250 mm
	Flange dimensions	:	OD 395 mm; PCD 350 mm,12x Ø22
	Impeller diameter (vanes)	:	625 mm
	Width in the impeller	:	130 mm
	Spherical pump passage	:	130 mm
Materials	: Pump casing	:	Ni-hard 4
	Impeller	:	Bainitic Nodular
	Wearing plate suction side	:	Ni-hard 4
	Shaft	:	42CrMo4
Hydraulics	: Drive	:	Hydraulic motor via a gearbox
	Maximum required oil flow	:	485 l/min. (continuous)
	Continuous required oil pressure	:	250 bar (delta p)
	Motor speed with this flow	:	Approx. 1,935 rpm
	Quick release coupling Snaptite:		
	Pressure	:	2” 75C32-32RP
	Return	:	2” 75N32-32RP
	Leak	:	1” 75N16-16RP
Pump performance	: Pump speed with max. oil flow	:	Approx. 900 rpm
	Max. available power at pump shaft	:	Approx. 195 kW
	Capacity DOP 250	:	See QH curves
Jet water	: Discharge connection	:	125 mm
	Flange dimensions	:	O.D. 250 mm; PCD 210 mm,8x Ø18
	Advised minimum available capacity	:	300 m^3/u, at 8 bar

Impeller : The impeller is of a closed type with 3 vanes and is statically balanced. It is secured on the impeller shaft by a torque coupling. Sense of rotation, seen to the suction side: **Clockwise.**

Sealing : An oil lubricated mechanical seal seals the shaft.

Working depth : Maximum working depth for the standard executed DOP pump is –50 meters. However, greater working depths are possible after special adjustments.

Execution :
- The suction pipe is provided with a suction mouth with 4 jetwater nozzles and a dirt grid or, alternatively with a flat suction head with jet water ring and dirt grid.
- A protective casing, made of steel, is surrounding the dredge pump and hydraulic motor.

- The hydraulic motor and gearbox are suitable for continuous operation under the water.
- The hydraulic oil has to be cooled by means of a cooler on the power pack.
- The hydraulic valve block with the necessary built-in safety valves, is mounted on the hydraulic motor and provided with quick release hose couplings and contra couplings.

Conservation : Shot blasted SA 2.5, 1 layer of primer and one top layer.

Tools : Impeller pressure piece, toolset mechanical seal, impeller hook.

Documentation : Instruction / maintenance manual in duplicate.

Maintenance : All pump parts are replaceable.

Transport dimension :
- Weight approx. 2,425 kg.
- L x W x H, approx. 3,700 x 1,550 x 1,250 mm.

Options :
- Suspension frame for the relieve of the (hydraulic) hoses.
- Hydraulically driven cutter unit or various other suction heads.
- Hydraulic hose set, flexible dredge hose and jet water hose.
- Diesel driven hydraulic power pack; or electrically driven.
- Jet water pump.
- Various dredging instrumentation.
- Various hoisting equipment.

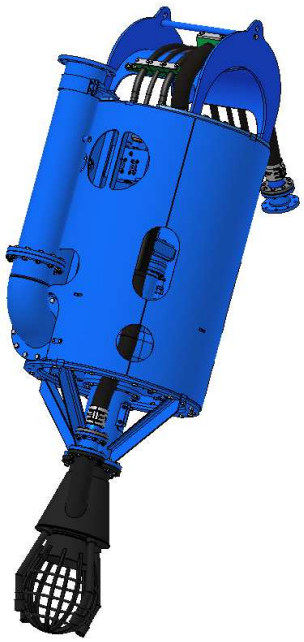

Damen Dredging Equipment
P.O. Box 1021
3860 BA Nijkerk
The Netherlands

Phone +31 (0)33 247 40 40
Fax +31 (0)33 247 40 65

E-mail info@damendredging.com
Website www.damendredging.com

DAMEN DREDGING EQUIPMENT

Prodredge report

ProDredge Project: DOP250-QH

Name	DOP250-QH
Client	Standard
Ship	DOP250
File	K:\Afdeling\Engineering\Afdeling\ProDredge\DOP\DOP250\DOP250-QH.prodred

Presentation: QH

Legend

Line		Situation	Conc %	Configuration	Speed(s) rpm	Prod m³/h
QH-900		Water (0,05mm)	0	DOP250	900	
QH-800		Water (0,05mm)	0	DOP250	800	
QH-700		Water (0,05mm)	0	DOP250	700	
QH-600		Water (0,05mm)	0	DOP250	600	

Explanation of pump curves

Configuration: DOP250

Element	Dept m	Lengt m	Diam. m	QH-900 kPa	QH-800 kPa	QH-700 kPa	QH-600 kPa
	0		0,25				
		0	0,25				
DOP250	0	0,2	0,25				
		0	0,25				
	0		0,25				

Pump	Type	Blade	Dimensions Øm x Øm x m	Drive	Nominal	Ratio
DOP250	BP2525M	3	0,3 x 0,6 x 0,1	DOP250 block	185kW @ 901rpm	1:1

Situation(s)

Name	Atmos. Pa	Temp °C	Water kg/m³	In Situ kg/m³	Grain kg/m³	d50 mm	Soiltype
Water (0,05mm)	101350	15	1000	1900	2650	0,05	Fine sand

Conditions of use

ProDredge 3.2 is a software product exclusively owned by Damen Dredging Equipment for the performance estimation of dredge systems. Actual performance is depending on the exact local circumstances and the proficiency of the operator. Calculations assume a free flowing mixture to the suction head that is not interrupted by any operational limitation. Performance guarantee can only be obtained for pumping water through signed consent from Damen Dredging Equipment. Damen Dredging equipment will not accept any responsibility for any damage (implied or consequential) or injury resulting from applying a dredge system as described in the calculation. Results are to be interpreted by experts in dredging technology. Damen Dredging Equipment will be available to assist in the evaluation of the results.

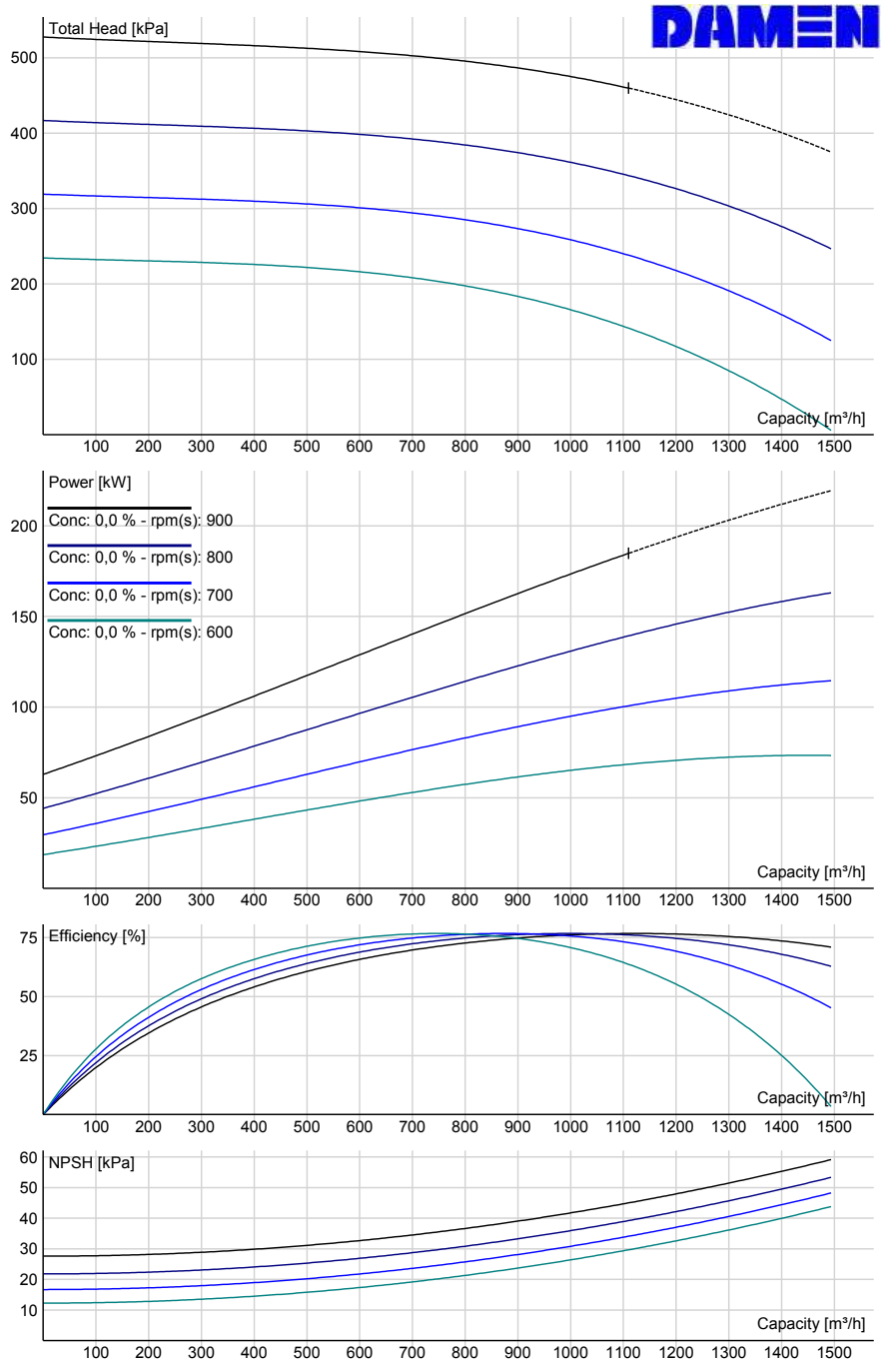
Total Head [kPa]
500
400
300
200
100
Capacity [m³/h]
100 200 300 400 500 600 700 800 900 1000 1100 1200 1300 1400 1500
Power [kW]
Conc: 0,0 % - rpm(s): 900
Conc: 0,0 % - rpm(s): 800
Conc: 0,0 % - rpm(s): 700
Conc: 0,0 % - rpm(s): 600
200
150
100
50
Capacity [m³/h]
100 200 300 400 500 600 700 800 900 1000 1100 1200 1300 1400 1500
Efficiency [%]
75
50
25
Capacity [m³/h]
100 200 300 400 500 600 700 800 900 1000 1100 1200 1300 1400 1500
NPSH [kPa]
60
50
40
30
20
10
Capacity [m³/h]
100 200 300 400 500 600 700 800 900 1000 1100 1200 1300 1400 1500

Production report: Production

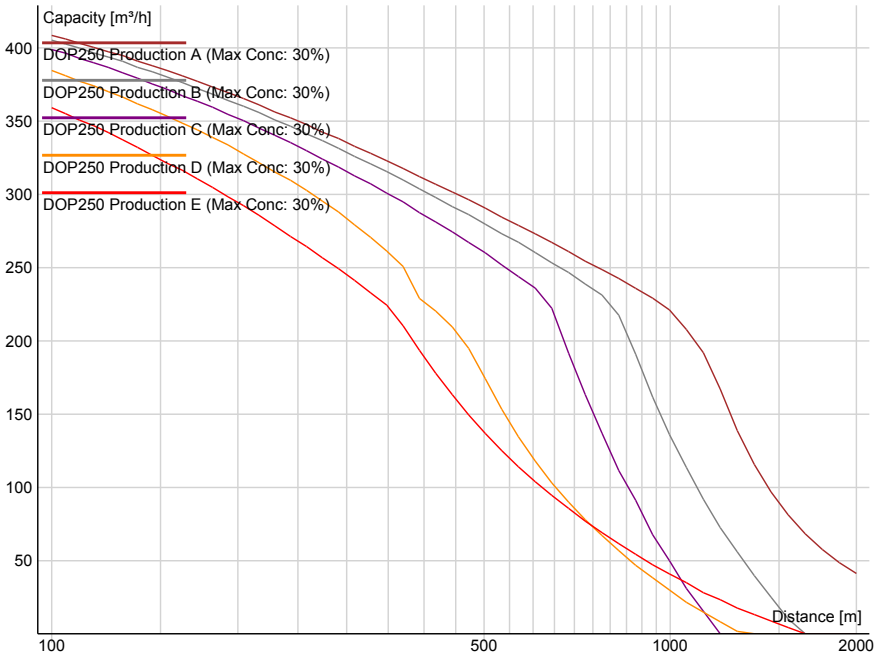

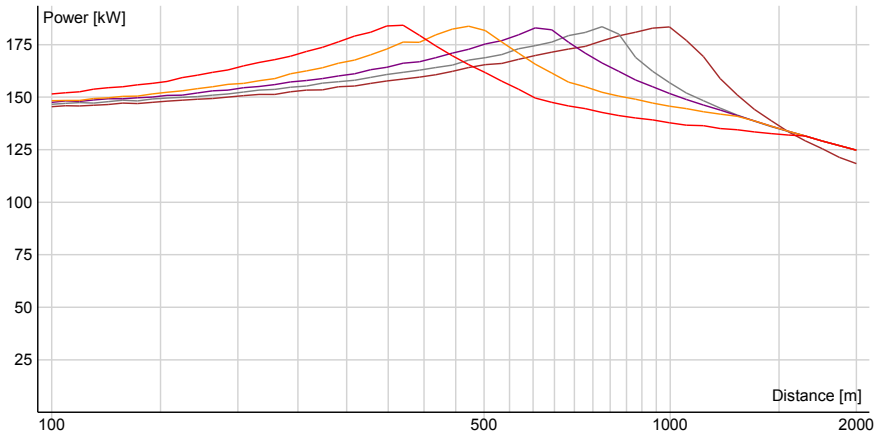

Name	Atmos. Pa	Temp °C	Water kg/m³	In Situ kg/m³	Grain kg/m³	d50 mm	Soiltype
A (0,11mm)	101350	15	1000	1900	2650	0,11	Fine sand
B (0,23mm)	101350	15	1000	1950	2650	0,23	Medium fine san
C (0,37mm)	101350	15	1000	2000	2650	0,37	Coarse sand
D (1,17mm)	101350	15	1000	2100	2650	1,17	Coarse sand an
E (2,37mm)	101350	15	1000	2100	2650	2,37	Gravel

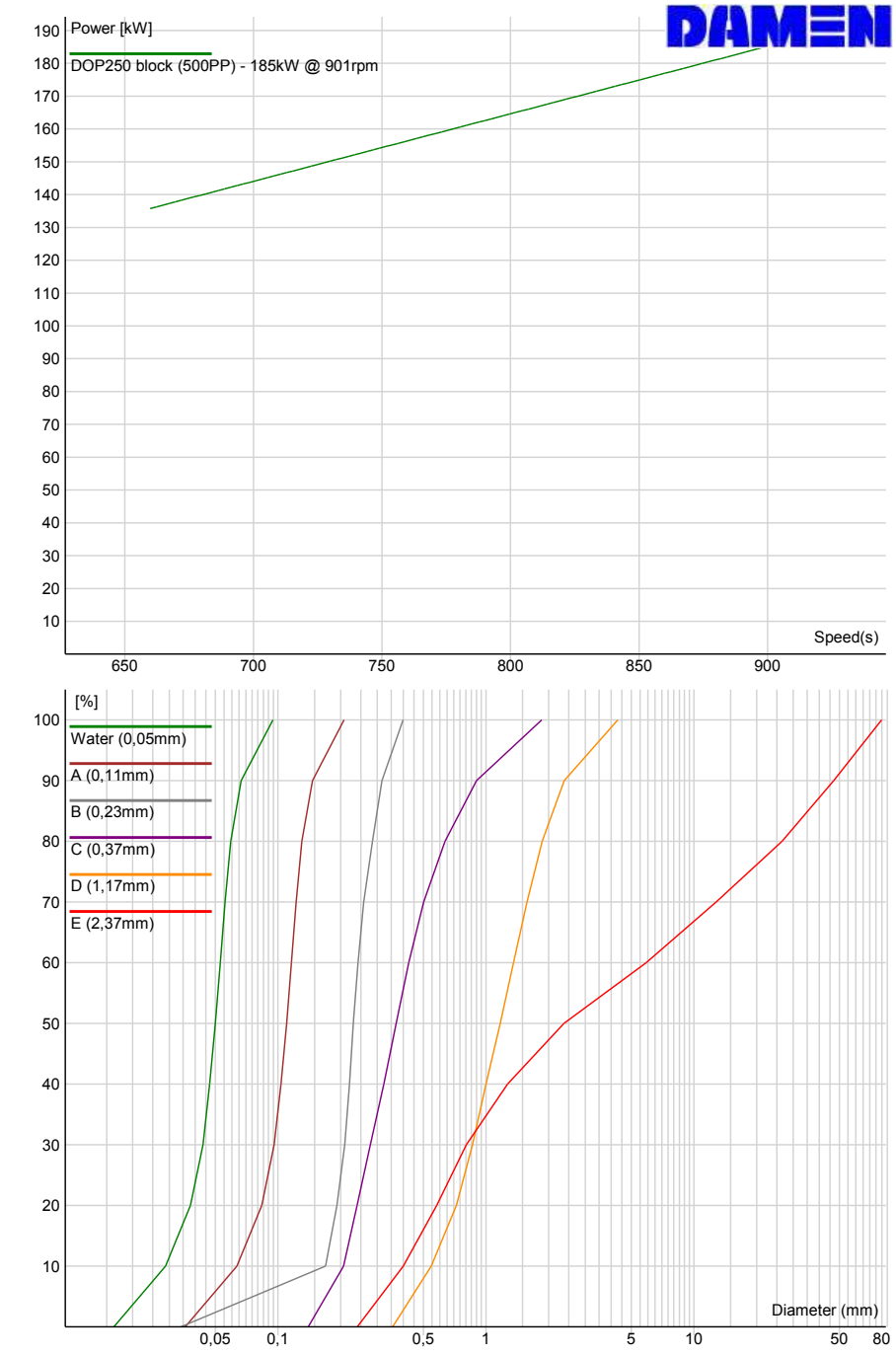
Power [kW]
DOP250 block (500PP) - 185kW @ 901rpm
190
180
170
160
150
140
130
120
110
100
90
80
70
60
50
40
30
20
10
650
700
750
800
850
900
Speed(s)
[%]
Water (0,05mm)
A (0,11mm)
B (0,23mm)
C (0,37mm)
D (1,17mm)
E (2,37mm)
100
90
80
70
60
50
40
30
20
10
0,05
0,1
0,5
1
5
10
50
80
Diameter (mm)

B

Trial-and-Error Method: Defining the Axial Gap width

As mentioned in section 6.1.10, an trial-and-error method can show the difference between a small or large axial gap width (s). The trail-and-error method is shown in the figures below, fig. B.1 shows the solution (not an exact solution, but an indication) for every dataset. For the other figures s is varied per figure for s is equal to $2mm$ to $20mm$ in steps of $3mm$, this is indicated in the figure itself.

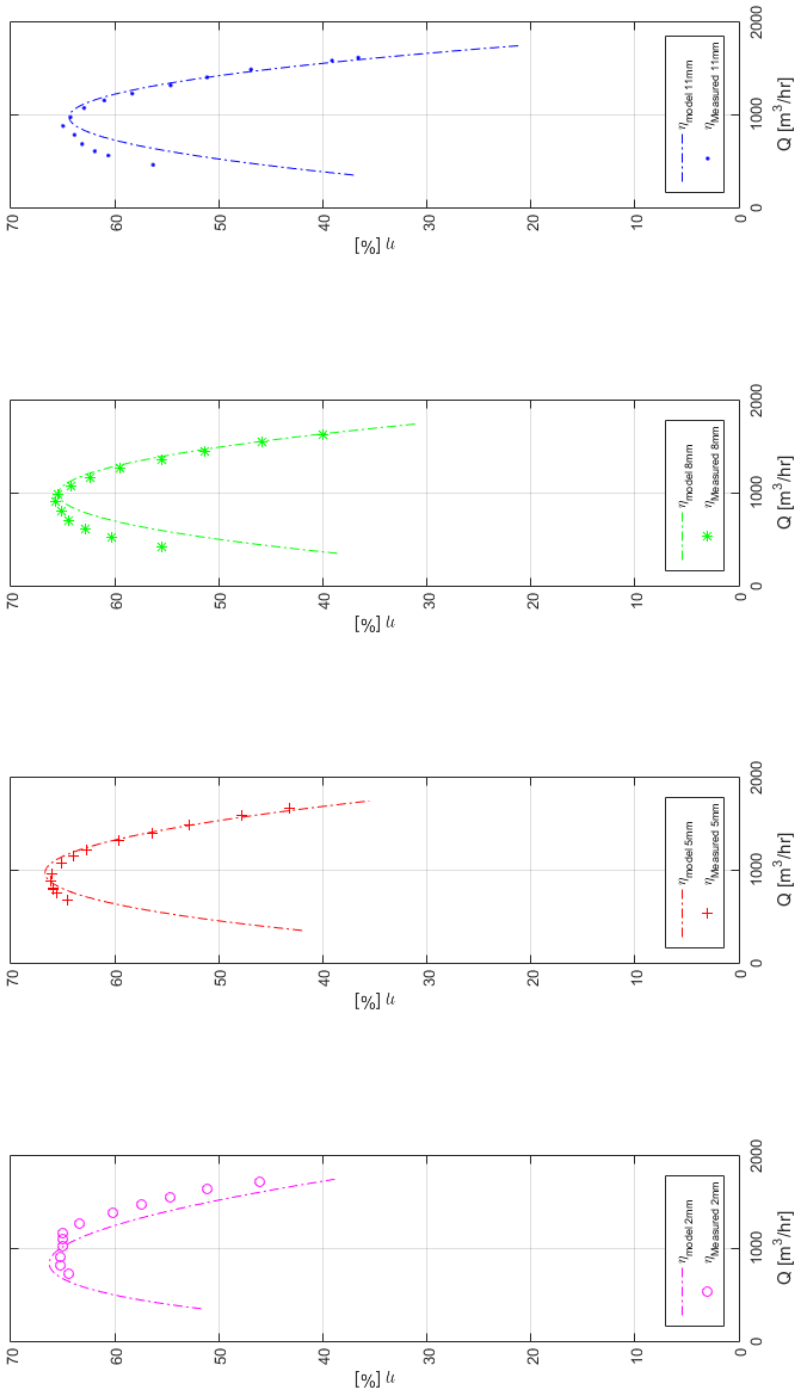

Figure B.1: Efficiency comparison between ($\eta_{Measured}$) and ($\eta_{model} \cdot C_{MDB}$) for the correct axial gap s per dataset [1]

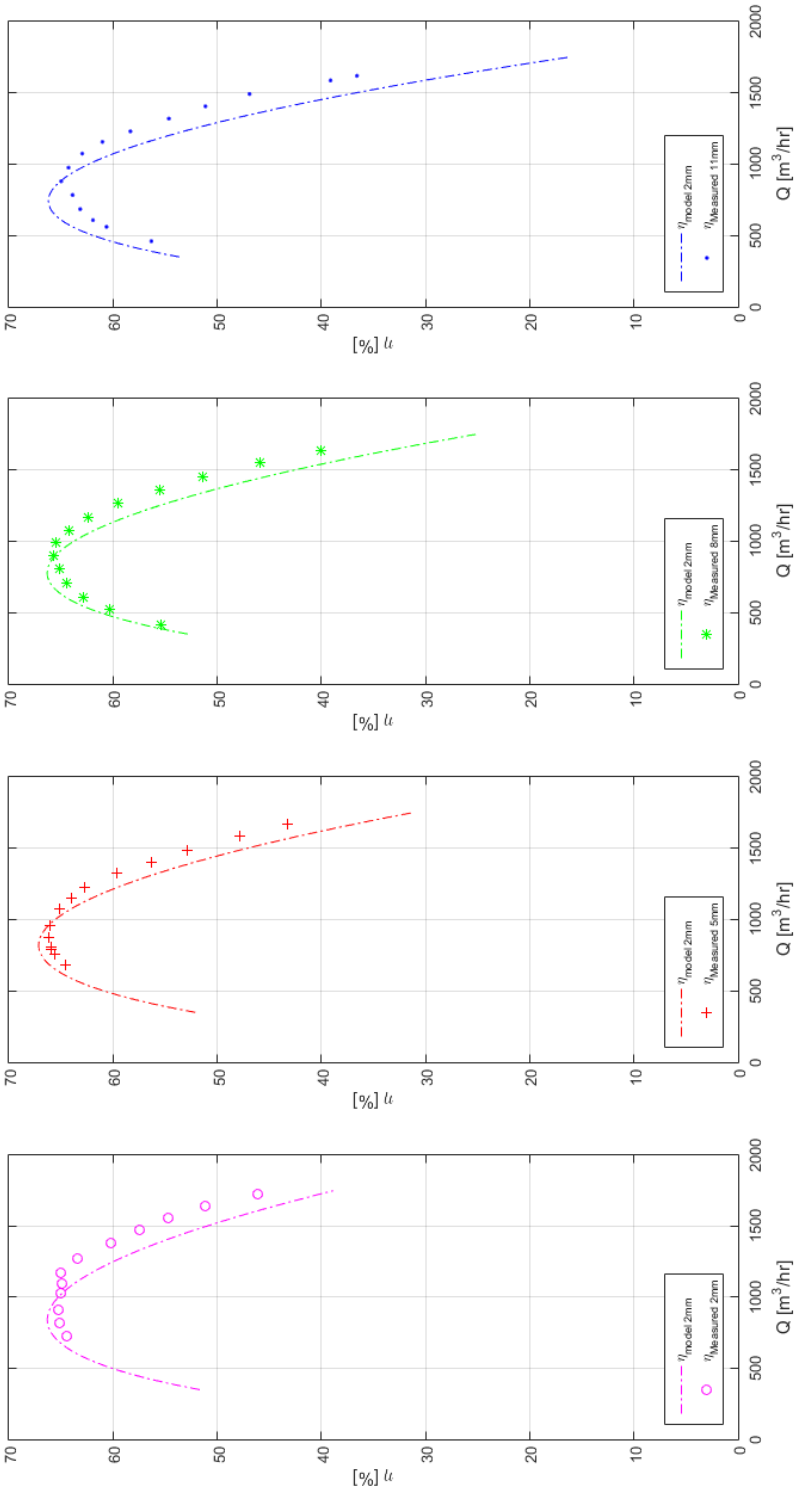

Figure B.2: Efficiency comparison between ($\eta_{Measured}$) and ($\eta_{model2mm} \cdot C_{MDB}$) [1]

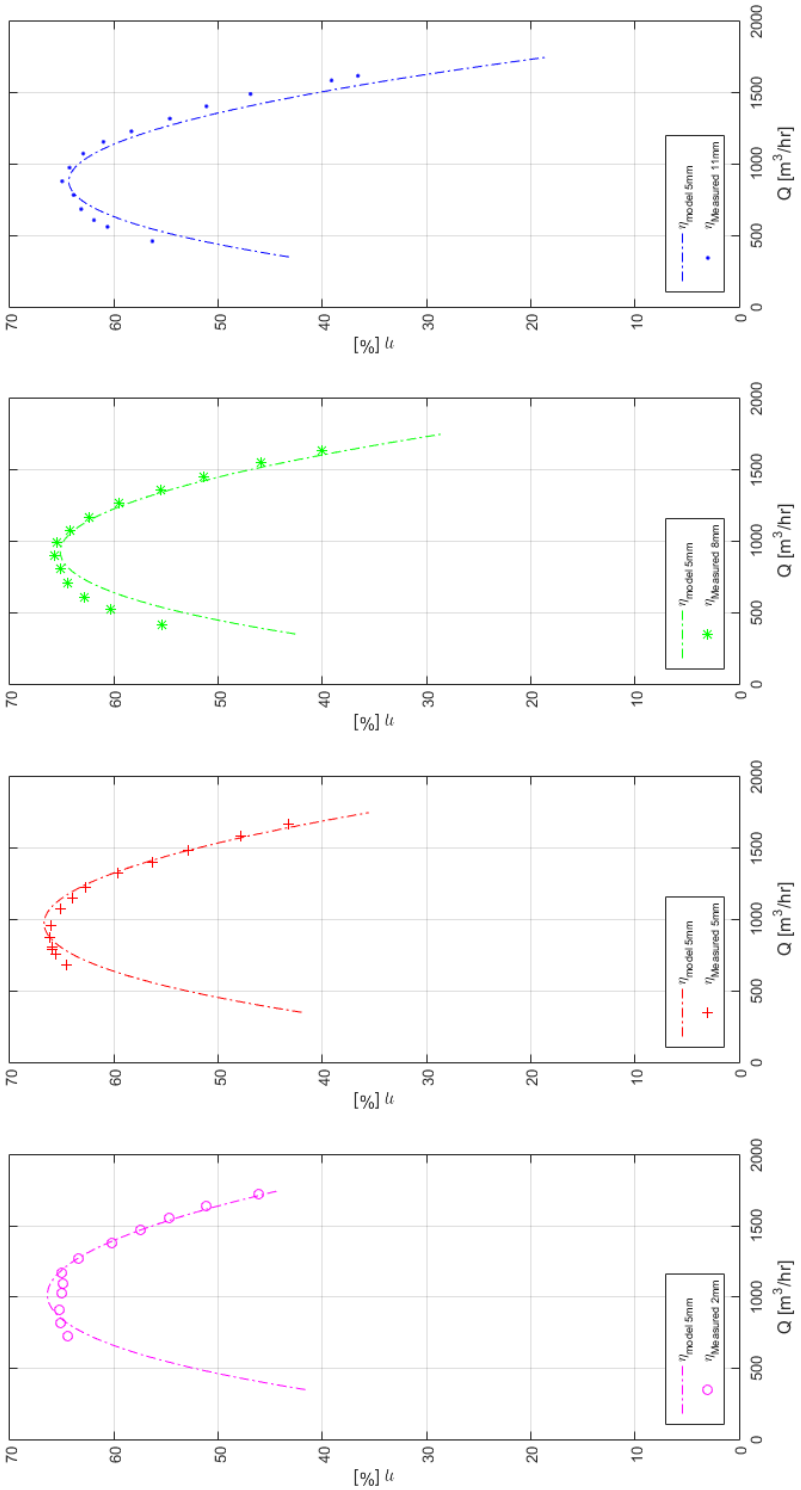

Figure B.3: Efficiency comparison between ($\eta_{Measured}$) and ($\eta_{model5mm} \cdot C_{MDB}$) [1]

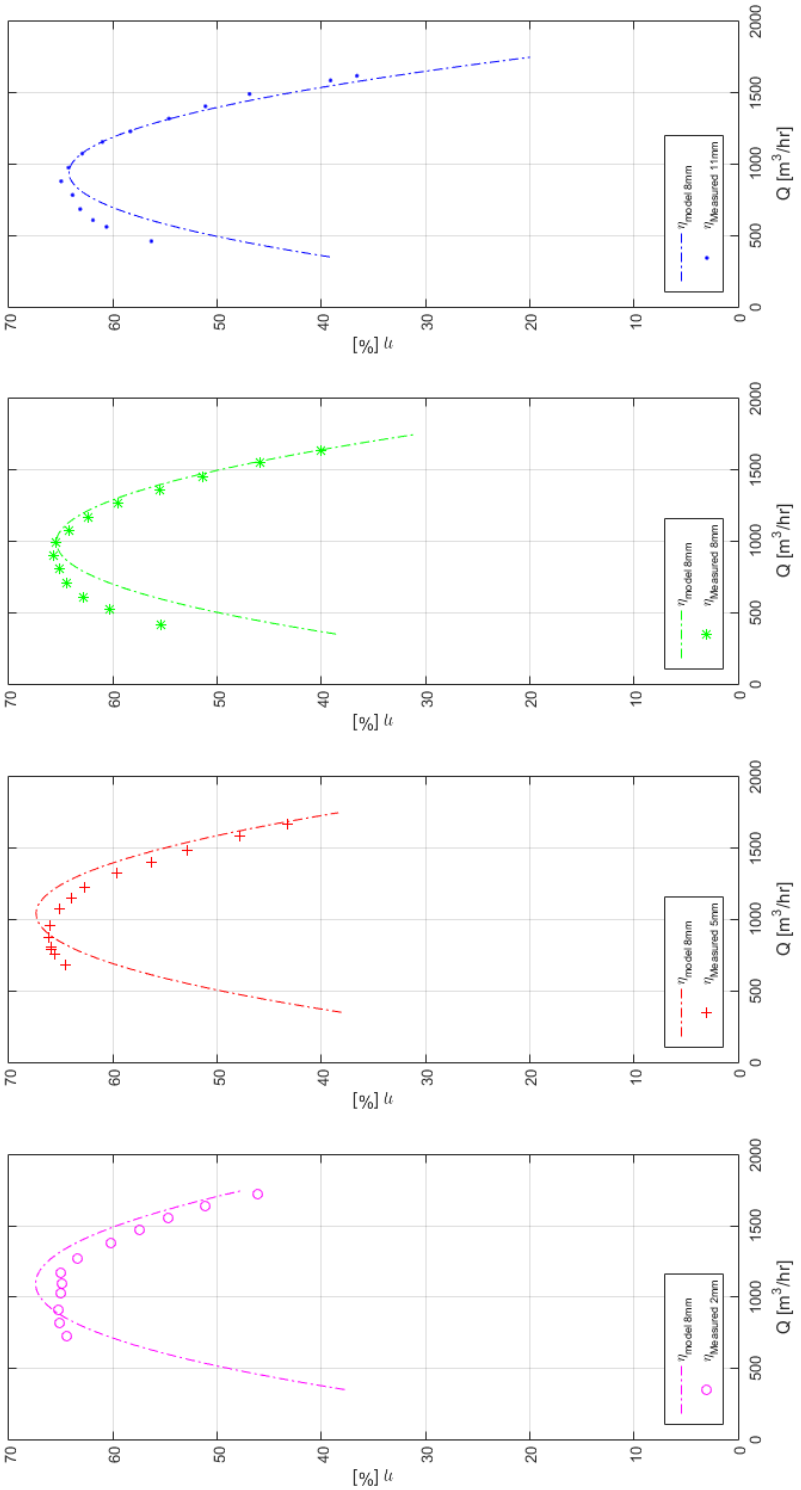

Figure B.4: Efficiency comparison between ($\eta_{Measured}$) and ($\eta_{model8mm} \cdot C_{MDB}$) [1]

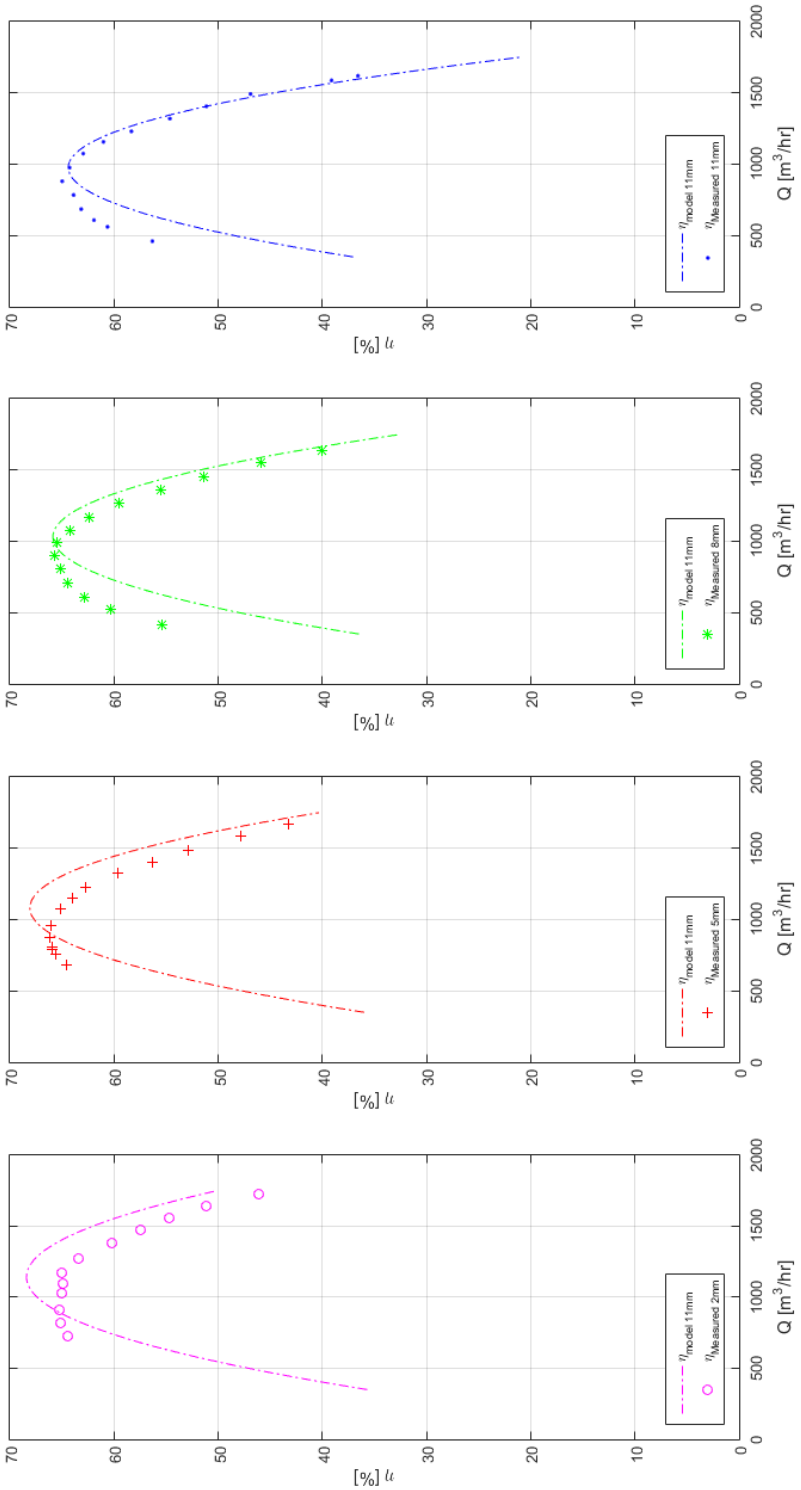

Figure B.5: Efficiency comparison between ($\eta_{Measured}$) and ($\eta_{model11mm} \cdot C_{MDB}$) [1]

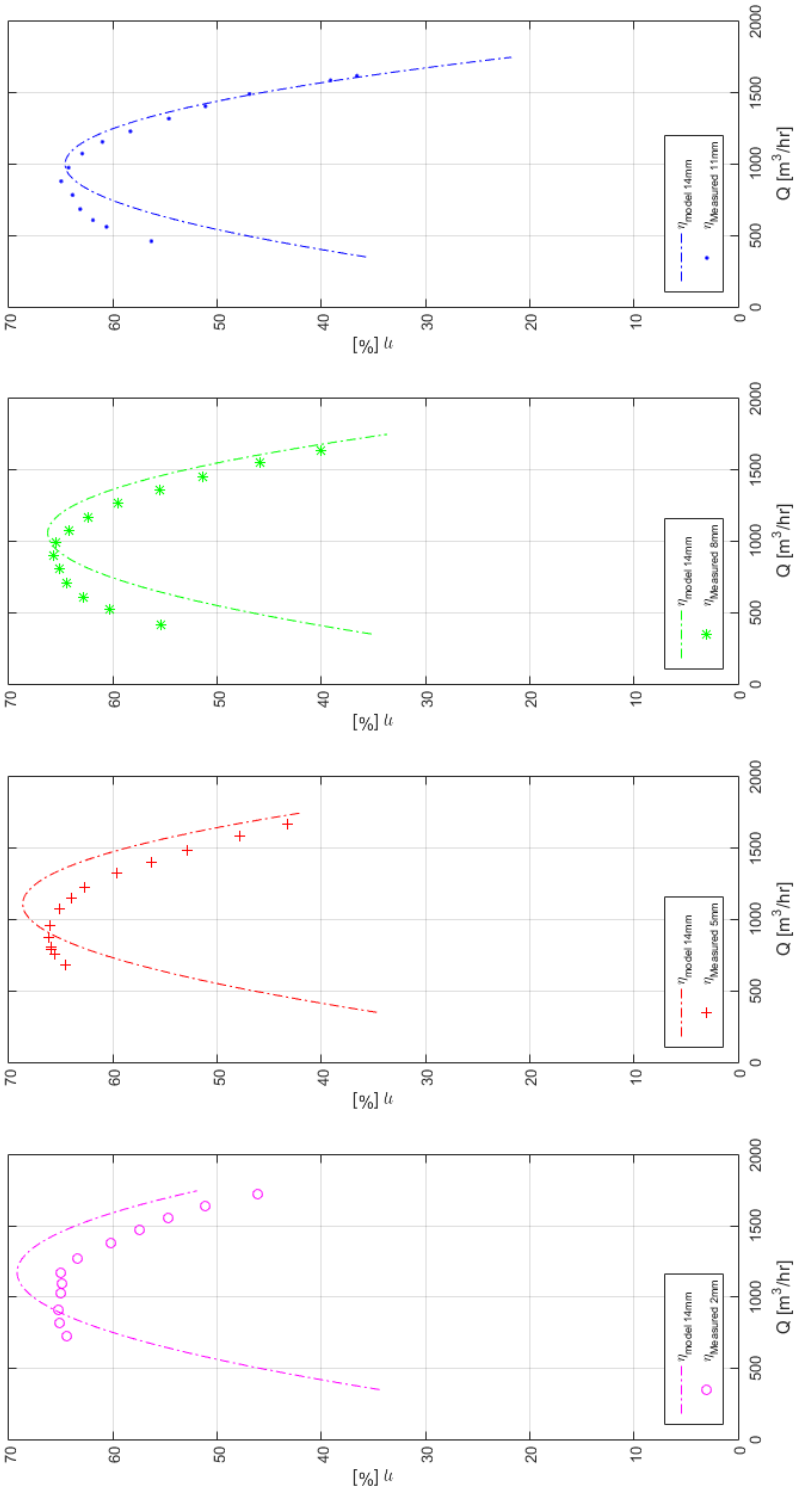

Figure B.6: Efficiency comparison between ($\eta_{Measured}$) and ($\eta_{model14mm} \cdot C_{MDB}$) [1]

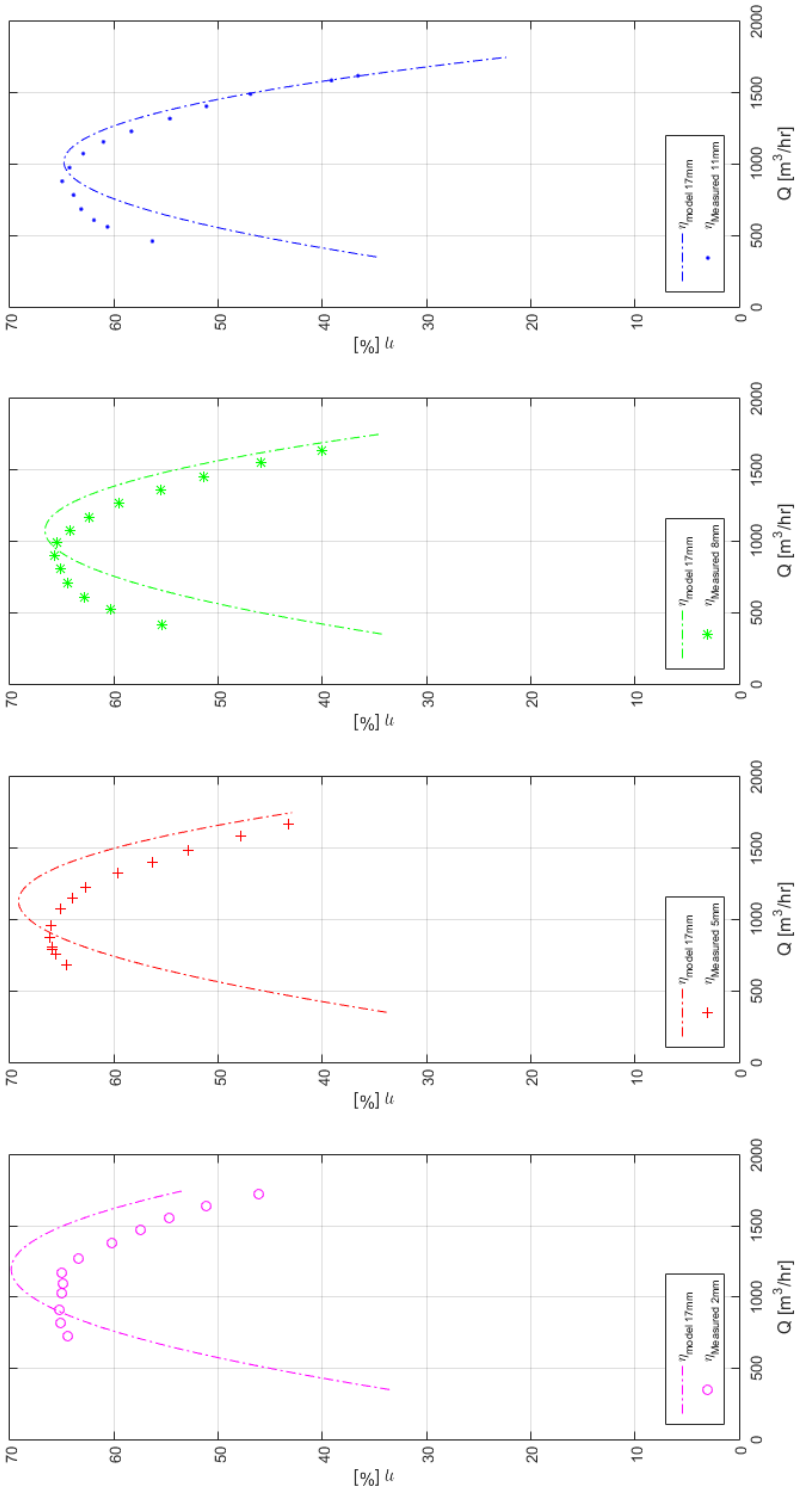

Figure B.7: Efficiency comparison between ($\eta_{Measured}$) and ($\eta_{model17mm} \cdot C_{MDB}$) [1]

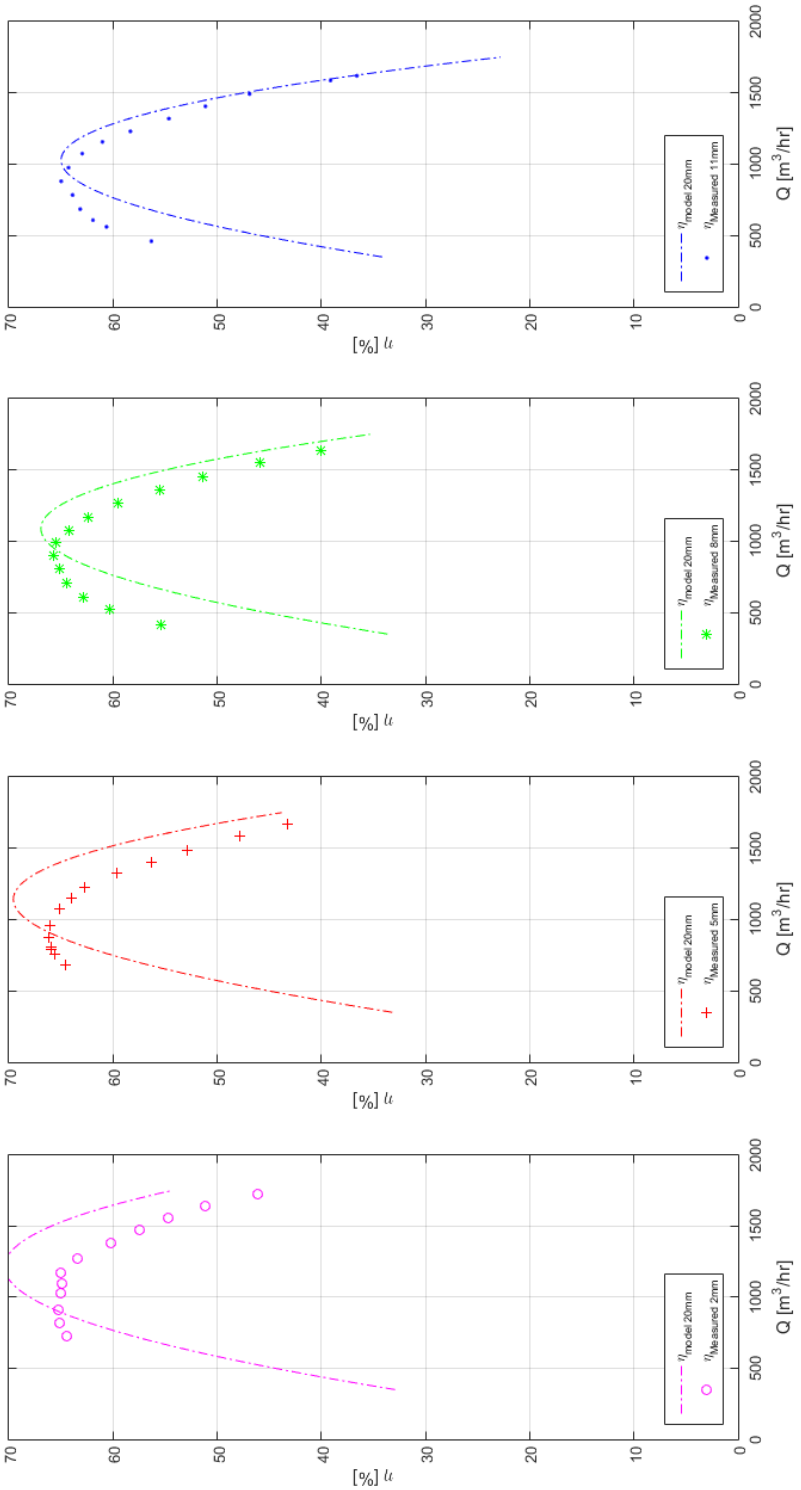

Figure B.8: Efficiency comparison between ($\eta_{Measured}$) and ($\eta_{model20mm} \cdot C_{MDB}$) [1]

BIBLIOGRAPHY

[1] W.L. Roorda & A. Frankema, *Process status evaluating tool,* Bachelor's thesis Hanzehogeschool Groningen (2015).

[2] Dr.ir.V.Matousek, *Lecture Notes Dredge Pumps and Slurry Transport* (Delft University of Technology, 2004).

[3] www.Grundfos.com, *The centrifugal pump,* (2016).

[4] V. C.G.Duan, *Abrasive Erosion & Corrosion of Hydraulic Machinery* (Imperial College Press, 2002).

[5] http://www.honstarslurry.com/, (2016).

[6] J. Tuzson, *Centrifugal Pump Design* (John Wiley & Sons, Inc., 2000).

[7] http://constructionmechanical engineering.blogspot.nl/, (2016).

[8] http://www.pumpsandsystems.com/, (2016).

[9] http://www.learnengineering.org/, (2016).

[10] A. K.C. Wilson, G.R. Addie, *Slurry Transport Using Centrifugal Pumps* (Springer, 2006).

[11] http://chemandy.com/calculators/round-wire-resistance calculator.htm, (2016).

[12] J. . M.Hodkiewicz, *Comparison of acoustic emission, vibration and dynamic pressure measurement for detecting change in flow conditions on a centrifugal pump,* (2005).

[13] P.G.O.Moniz, *Practical Centrifugal Pumps, Design, Operation and Maintenance* (Elsevier, 2005).

[14] J.F.Gülich, *Centrifugal Pumps* (Springer, 2014).

[15] A.J.Stepanoff, *Centrifugal and Axial Flow Pumps: Theory, Design, and Application* (John Wiley & Sons, Inc., 1948).

[16] A.Poullikkas, *Surface roughness effects on induced flow and frictional resistance of enclosed rotating disks,* Journal of Fluids Engineering (1995).

[17] A.Nemdili, *Development of an empirical equation to predict the disc friction losses of a centrifugal pump,* Tech. Rep. (Université des Sciences et de la Technologie d'Oran, 2004).